

EFFECTS OF KETAMINE ON NEURAL SIGNATURES OF PARKINSON'S DISEASE AND A NOVEL STRING-
PULLING BEHAVIOR QUANTIFICATION SYSTEM

by

Abhilasha Vishwanath

Copyright ©Abhilasha Vishwanath 2021

A Thesis Submitted to Faculty of the

DEPARTMENT OF PSYCHOLOGY

In Partial Fulfillment of the Requirements

For the Degree of

MASTER OF ARTS

In the Graduate College

THE UNIVERSITY OF ARIZONA

2021

THE UNIVERSITY OF ARIZONA
GRADUATE COLLEGE

As members of the Master's Committee, we certify that we have read the thesis prepared by: **Abhilasha Vishwanath**
titled: **Effects of ketamine on neural signatures of Parkinson's Disease and a novel string-pulling behavior quantification system**
and recommend that it be accepted as fulfilling the thesis requirement for the Master's Degree.



Stephen Cowen

Date: May 11, 2021



Andrew Fuglevand


Date: May 13, 2021



Torsten Falk

Date: May 12, 2021

Final approval and acceptance of this thesis is contingent upon the candidate's submission of the final copies of the thesis to the Graduate College.

I hereby certify that I have read this thesis prepared under my direction and recommend that it be accepted as fulfilling the Master's requirement. 



Stephen Cowen
Thesis Committee Chair
Psychology

Date: May 11, 2021



Acknowledgements

I want to acknowledge the National Institutes of Health R56 NS109608 funding that supported this project.

I would like to thank my advisor, Dr. Stephen. L Cowen, for his support, encouragement, expertise, and mentoring from day one. I would like to extend my thanks to my committee, Dr. Torsten Falk and Dr. Andy Fuglevand for their guidance.

I want to sincerely thank Dr. Mitchell Bartlett for being an invaluable resource and guide to me throughout this endeavor. I would also like to thank Gianna Jordan for her ingenuity, skill, and being an invaluable colleague.

Lastly, I want to thank my family whose support I cherish; without which I would not be here today.

Table of Contents

List of Figures	5
Abstract	6
Preface.....	8
Chapter 1	11
Introduction	11
Methods.....	22
Results	29
Discussion	46
Chapter 2	53
Introduction	53
Methods.....	56
Results	62
Discussion	65
Author Contributions	67
References	68

List of Figures

Figure 1.....	12
Figure 2.....	28
Figure 3.....	30
Figure 4.....	32
Figure 5.....	34
Figure 6.....	36
Figure 7.....	38
Figure 8.....	40
Figure 9.....	42
Figure 10.....	43
Figure 11.....	45
Figure 12.....	57
Figure 13.....	61
Figure 14.....	63
Figure 15.....	64

Abstract

The first part of the thesis reviews my investigations into the neural mechanisms underlying Parkinson's disease (PD) and levodopa-induced dyskinesia (LID) and their treatment with levodopa and ketamine. The second part of the thesis summarizes our group's development of a novel string-pulling behavior for assessing motor function in rodents.

Part 1: Parkinson's disease (PD) is a debilitating neurodegenerative disorder with motor and cognitive deficits. While levodopa is the leading treatment for PD, in many individuals long-term administration leads to Levodopa-Induced Dyskinesias (LID), which are uncontrollable involuntary movements. These side-effects are as debilitating as PD. A common neurophysiological feature of LID is the emergence of 80-Hz brain oscillations in the motor cortex. Ketamine, an FDA approved drug used in treating depression among other disorders and has been shown to alleviate LID symptoms in an animal model of LID. We used a unilateral 6-hydroxydopamine-lesion PD rat model to investigate the neural systems-level mechanisms of the effects of ketamine on LID. We found that ketamine administration was followed by reduced 80-Hz LID oscillations, increased gamma oscillations (~50 Hz), and reduced burst firing in individual neurons. One interpretation of these results is that ketamine triggers gamma activity that competes with and consequently reduces 80 Hz activity.

Part 2: The development of complex motor tasks and behavioral analysis is crucial for understanding the workings of motor neurons and study motor deficits. We developed a novel behavior quantification system for a bi-manual string-pulling task. The system has a unique

“infinite loop” and the capacity to simultaneously record neural activity. This integrated string-pulling system allows for investigation into the neural systems of motor behavior in healthy and disease populations.

Preface

Parkinson's disease (PD) is a neurodegenerative disorder that causes debilitating motor and cognitive deficits. It is the second most common neurodegenerative disease that affects in the US approximately 60,000 people per year with increased risk to people over 65 years of age (de Lau & Breteler, 2006). The cardinal motor symptoms experienced by patients are bradykinesia, rigidity of movement, and postural instability and tremors (Braak & Braak, 2000; Davie, 2008). This disease is the result of a substantial loss of dopamine neurons in the substantia nigra pars compacta (SNc) region of the brain (Lloyd & Hornykiewicz, 1970). Dopamine plays a vital role in initiating movement (Romo & Schultz, 1990), reward modulation (Mirenowicz & Schultz, 1994; Syed et al., 2015), muscle control (Crocker, 1997), motivation (Wise, 2004), and decision making (Egelman et al., 1998; Kurniawan et al., 2011). The significant loss of dopamine neurons in the SNc leads to a severe deficit in dopamine levels within several areas of the brain such as the basal ganglia, prefrontal cortex, motor cortex, etc. and leads to motor and cognitive impairments seen in PD. The most common and effective treatment available for PD is dopamine replacement therapy, specifically with the administration of Levodopa (L-DOPA) which is a precursor molecule for synthesizing dopamine. L-DOPA effectively alleviates most of the motor symptoms in PD patients. However, administration of L-DOPA for over approximately 5 years in patients diminishes its effectiveness (Davie, 2008) and leads to side effects. The most debilitating side effect of long-term administration of L-DOPA is known as Levodopa-Induced Dyskinesia (LID), which is a movement disorder that causes

involuntary movements (Jenner, 2008). LID can be as debilitating as PD itself. Thus, there is a dire need for more effective treatment for LID.

Ketamine is an FDA approved drug that is currently being used to treat depression (Duman et al., 2016), chronic pain (Reddi, 2016), migraines (Lauritsen et al., 2016), and post-traumatic stress disorder (Liriano et al., 2019). It has also been used as an anesthetic since the 1960s (Domino et al., 1965), and has shown to have neuro protective effects by increasing brain derived neurotrophic factors (Liu et al., 2012). Ketamine works as an *N*-methyl-D-aspartate (NMDA) receptor antagonist, among effecting other receptors like opioids receptors (Hirota & Lambert, 1996), and sub-anesthetic dose administration has recently been shown to reduce LID in preclinical studies (Bartlett et al., 2016, 2020). Ten-hour administration of ketamine in rats reduced dyskinetic behavior and was shown to have lasting effects for up to 24 weeks. Ketamine, however, has distinct and differentiated effects on neural synchrony and neuron modulation depending on the region within the brain (Ye et al., 2018), and although the drug has shown to be effective in clinical treatment of depression, the neural mechanisms by which it produces these effects are still unclear and largely unknown. In LID, 80 Hz oscillations emerge in both humans with PD and in animal models of PD, and ketamine has been shown to reduce these abnormal oscillations and to reduce LID symptoms. In the first chapter of this report, the effects of ketamine on neural mechanisms are explored in PD and LID rats using electrophysiology to assess the local field potential and single unit activity. The regions of interest are the primary motor cortex (M1), as it is strongly innervated by dopamine neurons

originating in the basal ganglia, and the dorsal striatum, as it receives primary dopamine input from the SNc.

The second chapter of this report will present a novel string-pulling task for quantifying complex motor behavior in rodents and the underlying neural correlates. The development of complex motor tasks is beneficial for understanding the neural underpinnings of coordinated movement. Moreover, it allows for assessment of motor deficits in PD. The tasks traditionally used to assess and diagnose motor dysfunction in rodents, such as rotating treadmill (Sabol et al., 1990) and vermicelli handling task (Allred et al., 2008; Tennant et al., 2010), do not allow for precise analysis of paw, hand, head, and body position. Detailed analysis of movement parameters may improve the understanding of motor deficits associated with different disease states. The string-pulling task offers a complex behavior that can be tracked and segmented in a precise format that is important for understanding M1 organization and classifying the motor symptoms in PD and other motor disorders.

Chapter 1

Ketamine's effects on LID and naïve rats: An electrophysiological study of single unit responses and changes in local field potential after ketamine administration

Introduction

Basal Ganglia function

The cortico-striato-thalamo-cortical loop is important for generating voluntary movement (Braak & Braak, 2000; Obeso et al., 2000), and the mechanisms of this loop and the basal ganglia circuitry is crucial for understanding the effects of dopamine denervation seen in PD. Significant loss of dopaminergic neurons in the SNc has an adverse impact on the functioning of the basal ganglia and the subsequent cortico-striato-thalamo-cortical loop. Axonal projections from the SNc are the major source of dopamine input to the dorsal striatum. The dorsal striatum, consisting of caudate and putamen, is the main input structure in the basal ganglia, and it projects to the globus pallidus interna (GPi) and substantia nigra par reticulata (SNr) through either the direct or indirect pathways (**Fig. 1**). The basal ganglia consist primarily of inhibitory medium spiny neurons that connect the structures. In the direct pathway, the striatum receives excitatory input through the activation of D1 dopamine receptor by dopamine from the SNc. The striatum then directly inhibits the GPi and SNr. The inhibition of these output structures leads to a disinhibition of the thalamus that increases excitatory input to the cortex, which ultimately supports movement. In the indirect pathway, the striatum is inhibited by the activation of D2 dopamine receptor by dopamine. The projections from the striatum go through

the globus pallidus externa (GPe) and the subthalamic nucleus (STN) before projecting onto the output structures. This pathway inhibits the GPe which, in-turn, inhibits the STN that decreases the excitatory input to the GPi and SNr. The reduced inhibition of the output structures results in increased inhibition from the thalamus creating a net decrease of excitatory output onto the

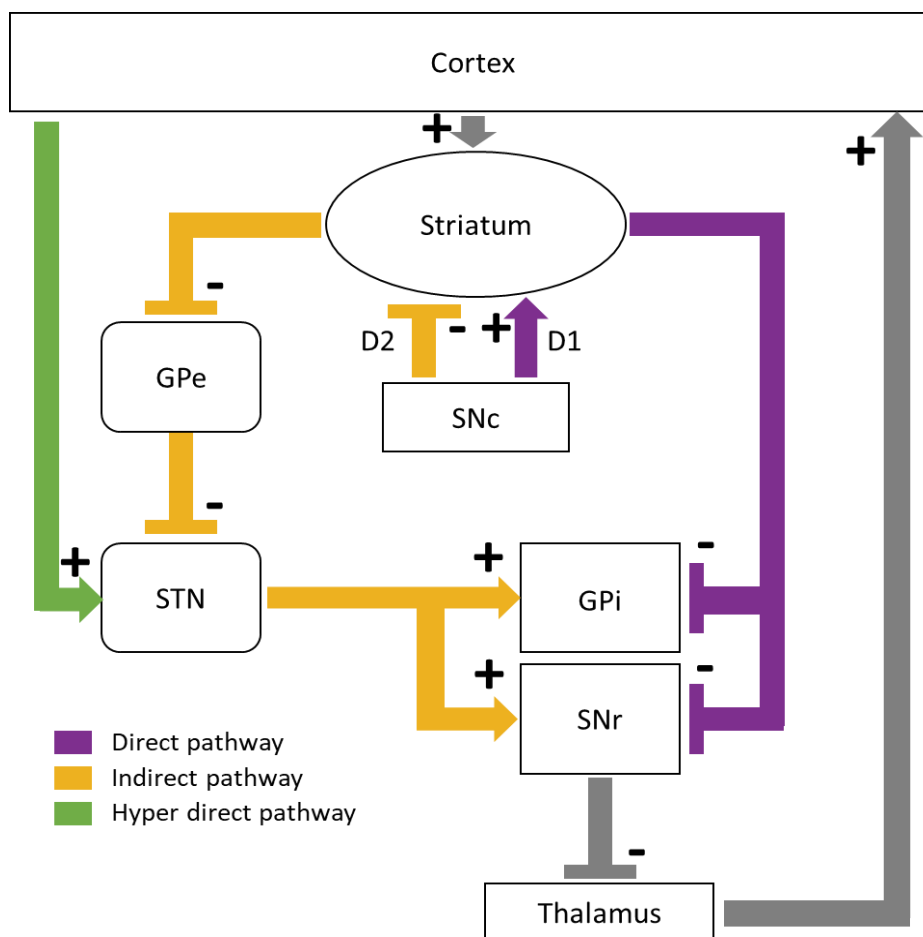


Figure 1: Basal ganglia circuitry in normal functioning. The '+' indicates excitatory inputs and '-' indicates inhibitory inputs. SNc: Substantia nigra pars compacta; GPe: Globus pallidus externa; STN: Subthalamic nucleus; GPi: Globus pallidus interna; SNr: Substantia nigra pars reticulata.

cortex (Jenner, 2008; Obeso et al., 2000).

Basal Ganglia dysfunction in PD and LID. During dopamine depleted conditions the traditional model of basal ganglia circuitry is disrupted. In PD, there is an increased inhibitory output from GPe in the indirect pathway along with a reduced excitatory input from the direct pathway (Jenner, 2008; Obeso et al., 2000). These disruptions lead to a net reduction in excitatory input to the cortex from the thalamus, thus leading to the motor deficits seen in PD. In LID, there seems to be a reversal of the excitation and inhibition of the pathways in the basal ganglia. The dyskinetic symptoms may be due to an excessive increase in the excitatory input from the direct pathway and a decrease in the inhibition from the indirect pathway (Jenner, 2008). This interpretation presumes the traditional model of the basal ganglia circuitry (**Fig. 1**); however, the mechanisms underlying LID do not always abide by this model (Obeso et al., 2000). The inhibitory output from the GPi onto the thalamus regulates voluntary movement. During LID, as per the traditional model, there is increased inhibition of the GPi thus disinhibiting the thalamus (Obeso et al., 2000). This excessive inhibition of the GPi through the direct pathway is modelled to be involved in generating involuntary dyskinetic movements. However, experiments using GPi lesions lead to an increase in dyskinetic movements rather than ameliorate the symptoms of LID, as the model suggests (Obeso et al., 2000). There has been other work showing that direct or indirect pathway stimulation alone is not enough to produce the dyskinetic behavior seen with L-DOPA administration (Alcacer et al., 2017). Other work suggests that the pattern of neural firing from the basal ganglia, rather than overall excitation or inhibition, may be more informative in understanding the development of dyskinetic movements (Obeso et al., 2000).

Oscillatory and individual neural activity in PD and LID

Brain oscillations are rhythmic and synchronous neural activity that have been shown to be indicative of abnormal and normal brain states (Little & Brown, 2014). Oscillations occur in multiple frequencies, ranging from 0.5-500 Hz (Buzsaki, 2004), and certain frequencies are specific to brain regions and are correlated with neural activity and the corresponding behavior. Synchronized oscillations can be computationally advantageous as they can organize the activities of ensembles of neurons to optimize information flow between and within brain regions (Buzsaki & Wang, 2012; Jenson & Colgin, 2007; Little & Brown, 2014). However, excessive synchrony can also limit the information processed by populations of neurons, thereby inhibiting the informational flow (Little & Brown, 2014), for instance hypersynchrony in neural circuits that are the basis for epileptic seizures (Rao & Lowenstein, 2015).

Beta oscillations and PD. The debilitating motor symptoms of PD correspond to an increase in local field potential (LFP) oscillations in the beta band frequency (15-35 Hz) in M1 (Hammond, Bergman & Brown, 2007) and in subcortical structures (Weinberger et al., 2006). The increase in beta oscillations in M1 has been correlated with both reduction in dopamine levels in basal ganglia structures and decreased ability to initiate voluntary movements (Brown, 2007; Kuhn et al., 2009). The administration of L-DOPA and other dopamine agonists have been shown to reduce M1 and subcortical beta oscillations (Jenkinson & Brown, 2011). The mechanisms that generate beta oscillations are unclear. It has been shown that there is increased beta-band coherence in the LFP between M1 and the STN, GPe and the striatum

(Little & Brown, 2014). Increased beta-band coherence in dopamine-depleted states may indicate that there is increased synchrony between the two brain regions where M1 activity entrains activity in the basal ganglia (Little & Brown, 2014). Thus, increased transmission between cortex and basal ganglia may sustain oscillations seen in disease states (Brazhnik, 2012).

80 Hz gamma oscillations in LID. The oscillatory signatures of LID have been reproduced consistently in animal models of PD and seen in human patients. During dyskinetic states, there is an emergence of a narrow band 80-Hz gamma oscillations in M1 seen in animal models that are unique to this motor dysfunction (Halje et al., 2012). These oscillations are correlated with the dyskinetic behaviors seen in animal models of PD (Halje et al., 2012) and in human patients (Brown et al., 2001). In human patients, 80 Hz oscillations have been recorded in the STN from deep brain stimulation electrodes (Brown et al., 2001). The 80 Hz oscillations were so well titrated to the dyskinetic behavior that it has been speculated to be causal to generating the abnormal movements (Halje et al., 2012). A more recent study, however, has shown that the emergence of 80 Hz oscillations is dependent on the L-DOPA dosage and priming, suggesting that significant dyskinetic symptoms can appear in the absence of 80 Hz (Ye et al., 2021). The single-unit activity study by Halje et al. found only 12% of pyramidal cells and 18% of interneurons in M1 that were phase modulated to the 80 Hz, unlike the beta oscillations where M1 neurons are significantly modulated to the phase of the beta oscillations (2012). Spike entrainment to oscillations is indicative of local neural ensemble activity involved in generating

the oscillation. However, there are not a lot of studies, to our knowledge, looking at extracellular single unit activity in the cortex during the 80 Hz oscillation in LID animals (Halje et al., 2012). The spike entrainment to 80 Hz would shed light on the networks involved in generating these narrowband oscillations, the cortico-striato-thalamo-cortical loop involvement, and role of dopamine denervation.

Ketamine's mechanism of action

Ketamine has been used as an anesthetic since the 1960s (Domino et al., 1965). In the last decade, ketamine has gained a lot of attention as a treatment for depression (Berman et al., 2000; Duman et al., 2016), migraines and chronic pain (Lauritsen et al., 2016; Reddi, 2016), mediation of synaptic plasticity in depressive patients with stress related atrophy (Duman et al., 2016). Ketamine's short-term effects are shown to be mediated by the NMDAR blockade, but its long-lasting effects on depression and plasticity changes are thought to be mediated through facilitating glutamate release and alpha-amino-3-hydroxy-5-methylisoxazole-4-propionic acid (AMPA) receptor function (Fukumoto et al., 2016; Li et al., 2010), increased signaling of rapamycin target protein (m-TOR) pathway and brain derived neurotrophic factor production (Duman & Aghajanian, 2012; Li et al., 2010). It has been recently shown that ketamine's ability to induce both the early and late effects may be tied to increased dendritic spine density in pyramidal cells (spinogenesis) through dopamine mediated mechanisms in the medial prefrontal cortex (Wu et al., 2021). Ketamine may also induce plasticity changes by increasing the density of dendritic spines (Duman & Aghajanian, 2012). Low-dose ketamine has been

shown to promote the growth and development of dendritic spines in the cerebral cortex (Wu et al., 2021) and increase synaptic signaling and functions of newly formed synapses in the PFC through the mTOR pathway (Duman & Aghajanian, 2012; Wu et al., 2021). These findings allude to mechanisms underlying neurodegenerative disorders that are directly related to ketamine's effects on the brain.

Ketamine mediated oscillatory activity

Spontaneous gamma activity has been shown to emerge after ketamine administration in rodent studies (Lazarewick et al., 2010; Pinault, 2008;), non-human primates (Slovik, 2017), and some studies in human subjects (Shaw et al., 2015) in several brain regions. Gamma oscillations seen in M1 after ketamine have been correlated with increased movement in rodent studies (Crone et al., 1998; Pfurtscheller et al., 2003). However, ketamine's effects on LFP and neural populations in the cerebral cortex stem from models for schizophrenia (Krystal et al., 1994). The role of NMDA receptor (NMDAR) hypofunction and increased gamma activity seen in schizophrenic patients led to the use of ketamine to predominantly mimic the positive symptoms of schizophrenia (McNally et al., 2011). As mentioned before, gamma oscillations (35-40 Hz) have been tied to GABAergic parvalbumin (PV) inhibitory interneurons in the cortex (Cardin et al., 2009). PV interneurons work to modulate the inhibition and excitation of the pyramidal cells (Kocsis, 2012; Ferguson & Gao, 2018) and are critical for generating the narrowband gamma oscillations. Ketamine has been shown to mediate broadband gamma activity (30 – 80 Hz) through the blockade of NMDARs on PV interneurons (Guyon et al., 2021).

While PV interneurons are involved in generating narrowband gamma, inhibiting PV cells does not obliterate gamma oscillations, but in-turn systemic inhibition of PV interneurons increases broadband gamma activity (Guyon et al., 2021). Work from Carlen et al., suggests the importance of NMDAR function in PV interneurons for synchronous gamma oscillations and spike entrainment to gamma (2012).

Ketamine induces unique patterns of oscillatory activity in different brain regions. For example, in the experiment conducted by Ye et al, acute and repeated ketamine injections induced high frequency oscillations (HFOs: 120-160 Hz) in the striatum, broadband activity (> 30 Hz) in the hippocampus, and gamma activity (35-55 Hz) in M1 (2018). They found that ten-hour exposure to intermittent ketamine administration produced an increased power in the gamma, HFO, and broadband activity in M1, striatum, and hippocampus respectively as a function of ketamine administration. Ketamine has also shown to increase theta-gamma cross frequency coupling and delta-HFO coupling (Ye et al., 2021). Cross-frequency coupling is the phenomenon where a faster oscillation occurs consistently at a particular phase of a slower oscillation (Bragin et al., 1995; Jenson & Colgin, 2007; Dvorak & Fenton, 2014). This cross-frequency modulation has been shown to facilitate synchronization between and within brain regions to optimize information flow (Jenson & Colgin, 2007). In addition, a D1 receptor antagonist given with ketamine has been shown to reduce both gamma activity and movement (Ye et al., 2018) suggesting an involvement of dopamine during ketamine's action.

Single unit activity during ketamine

Ketamine administration has been shown to increase both pyramidal cells and interneurons activity in the cortex (Guyon et al., 2021; Shen et al., 2018). Despite increasing overall firing rate of cells (Guyon et al, 2021), ketamine reduces burst firing of neurons (Yang et al., 2018). Burst firing is the phenomenon where neurons fire with short latency periods between consecutive spikes followed by a silent period before firing another burst of action potentials (Johnson, Seutin & North, 1992; Lisman, 1997). Previous studies have shown that burst firing is important for increasing the probability of information transmission between cells as the probability of post synaptic depolarization is increased due to the high frequency bursts (Lisman, 1997). It has also been speculated that burst firing transmits informationally rich content (Lisman, 1997). Burst firing, however, has been shown to be enhanced in certain regions of the brain in depressive states (Yang et al., 2018). Yang et al. found that the rapid anti-depressive effects of ketamine may be due to the targeted reduction in burst firing in the lateral habenula region in depression (2018).

Ketamine and LID

The case study by Sherman et al. with PD patients found a significant reduction in dyskinesia lasting weeks following two to three day low-dose ketamine infusions (2016). This anti-dyskinetic activity was also shown in a rat model of established LID, and the effect of a single ten-hour ketamine treatment lasted for over 50 days (Bartlett et al., 2016). A recent preclinical study (Bartlett et; al., 2020) has shown that ketamine reduces development of LID

symptoms in rat models of PD. Ketamine-treatment in LID animals also reduces 80 Hz activity associated with dyskinesia in M1, dorsomedial striatum (DMS), and nucleus accumbens (NAc) (Ye et al., 2021). Acute ketamine administration induced a broadband gamma oscillation in M1 and HFO in DMS and NAc during the disruption of 80 Hz activity which was correlated with reduced AIMs scores during ketamine's active period.

Present study

Given ketamine's association with LID motor symptoms and oscillatory activity, our study investigates ketamine's effects on LFP and single unit activity in a LID rodent model and naïve rats with acute ketamine injections. We used unilateral 6-hydroxydopamine-lesioned (6-OHDA) rat model of PD and induced LID by treating the animal daily with L-DOPA (12 mg/kg for ≥ 10 days). The 80 Hz gamma and the lower frequency gamma (~ 50 Hz) seem to be generated by distinct cortical circuits (Buszaki & Wang, 2012). The circuits that are involved in generating gamma can be divided into the inhibitory interneuron to interneuron (I-I) model and the pyramidal cell to interneuron (P-I) model (Buszaki & Wang, 2012). The fast-spiking interneurons are more likely to be involved in generating high gamma oscillations (Brunel & Wang, 2003), thus the 80 Hz oscillations in LID might be generated from I-I activation and the ketamine induced gamma (~ 50 Hz) might be generated from the P-I activation. Thus, we hypothesize that ketamine will decrease the LID 80 Hz oscillations in LID animal by generating competing lower frequency gamma in M1. We also predict that ketamine will decrease dyskinetic behaviors based on findings from previous studies (Bartlett et al., 2016, 2020; Ye et al., 2021). With

ketamine administration in naïve and PD animals (without L-DOPA administration), we predict to see the spontaneous gamma oscillations and the HFOs, as shown previously (Ye et al., 2021), in both M1 and the striatum.

With our single-unit analysis, we hypothesize that the neurons would phase lock to the oscillations induced by LID and ketamine in M1. The spike phase locking to the 80 Hz oscillations were shown to our knowledge in only one previous study (Halje et al., 2012). We predict that we will find a subset of M1 neurons that reliably fire at certain phases of the 80 Hz oscillations in the lesioned hemisphere but not the un-lesioned hemisphere of LID rat.

Ketamine has been shown to reduce burst firing (Yang et al., 2018) and studies show that there is increased burst firing in PD and LID animals (reviewed in Ellens & Leventhal, 2013), specifically in the GPe, STN, and thalamus. We hypothesize that ketamine will reduce burst firing in M1 and striatum, and L-DOPA administration will increase burst firing. Specifically, we predict that neurons will reduce bursting in a naïve animal in both M1 and striatum. For the LID animal we restricted our analysis to M1 due to the low neuron count in the striatum. In M1 of PD animal we predict that neurons will reduce burst firing post ketamine administration. In the dyskinetic animal, i.e., when given L-DOPA, we predict to see an increase in burst firing post L-DOPA and a subsequent reduction in burstiness upon ketamine administration.

Lastly, for the firing rate changes in M1, we know that ketamine might affect the interneurons and pyramidal cells differently due to the different concentration of NMDA receptors on these cell types. However, in this study, we look at the firing rate of all recorded

neurons post ketamine or L-DOPA administration. We predict that ketamine would increase the firing of neurons. This hypothesis is driven by the fact that our dataset might contain more pyramidal cells than interneurons as interneurons only make up 10-15% of cortical cells and have lower-amplitude waveforms which makes them more difficult to resolve from extracellular electrodes. Additionally, the increase of firing might be due to the disinhibition effect on pyramidal cells by the inhibition of interneurons by ketamine. The inhibitory interneurons maintain a tonic inhibition onto the excitatory pyramidal cells (Buzsaki & Wang, 2012). Thus, ketamine's action on the interneurons could cause a disinhibition of the excitatory pyramidal cells. Our future analysis will separate putative interneurons from pyramidal cells based on waveform shape and firing rate of the neurons.

Methods

Animals

Male Sprague-Dawley rats (n = 2, 280-320 g at arrival, Envigo, Indianapolis, IN, United States) were housed individually in a 12-h reverse light/dark cycle (i.e., lights off from 9AM to 9PM) room with food and water available *ad libitum*. The rats were divided into two groups: control (n = 1) and LID (n = 1). All procedures were in accordance with NIH guidelines for the Care and Use of Laboratory Animals and approved IACUC protocols at the University of Arizona.

Unilateral 6-OHDA-lesion PD model

As previously published (Bartlett et al., 2016), 6-OHDA hydrochloride (5 $\mu\text{g}/\mu\text{l}$) was injected into 2 locations (12.5 $\mu\text{g}/\text{site}$) of the medial forebrain bundle: MFB: AP = -1.8 mm, ML= +2.0 mm, DV= -8.2 mm, and AP = -2.8 mm, ML= +1.8 mm, DV = -8.2 mm. Amphetamine-induced (5.0 mg/kg, i.p., Sigma-Aldrich) rotations were scored by blinded experimenters to assess the degree of lesion. An average score ≥ 5 corresponds to $>90\%$ dopamine depletion (Dekundy et al., 2007). The rat included in the study met the above criteria.

Drug treatments and dyskinesia scoring

Dyskinesia was induced in the 6-OHDA-lesioned rats by daily administration for a period of 10 days (**Fig. 2a**) with L-DOPA (12 mg/kg) + benserazide (15 mg/kg, i.p., Sigma-Aldrich). During recording sessions ketamine was administered i.p. using a 20 mg/kg solution.

The severity of LID was scored using previously described abnormal involuntary movement (AIM) measurements (Dekundy et al., 2007) with modifications specified in Bartlett et al., 2020. Rats were scored for dyskinesia after the 10-day priming and only rats with severe dyskinesia scores were implanted with micro-drives. Dyskinesia was scored during all L-DOPA administration sessions post implant. A maintenance dose of L-DOPA (12 mg/kg) was given every 3-4 days post priming to maintain dyskinetic effects throughout the experiment. There was a period of at least 48 hours with no drug treatments prior to any recording session for LID animal. If L-DOPA was given during a recording session the maintenance dose was skipped for that cycle.

Drive implantation

Drive implant surgeries were performed using isoflurane (1.5–2.0%; VetOne, Boise, ID) anesthesia. Dual bundle micro-drive with 16 movable tetrodes (8 tetrodes in each bundle; NeuroTek, Toronto, Ontario, Canada) were implanted in left and right primary motor cortex (center coordinates: AP = +1.5mm, ML = +2.2mm, DV > -2.5mm from bregma and brain surface) and moved into the striatum (DV < -3 mm). A skull screw over cerebellum was reference and ground. The tetrodes were moved 15 to 20 hours before every unique recording session. Rats were allowed to recover for 1 week before testing.

Neural recordings

Data was acquired from a multi-channel recording system (INTAN RHD USB Interface Board, INTAN Technologies, Los Angeles, California, United States). The signal from the animal was transmitted using a light-weight tether attached to the digitizing head-stage connected to the animal. A colored sphere was attached to the drive of the rat for tracking movement (Camera: Manta G-033C, Allied Vision, Exton, PA, United States). Recordings were conducted in a faraday cage (47 X 55 cm). If the animal was doing behavior tasks (string-pulling or rotating treadmill tasks) it was done prior to the baseline period before any drug treatments.

Histology

Current stimulation (20 μ A for 10 sec) was used to make electrolytic lesions at tetrode locations. Rats were injected with Euthasol (0.35 mg/kg, i.p.; Virbac, Fort Worth, TX), after three days following lesions, and perfused using 0.9% saline and phosphate buffer 4%

paraformaldehyde. Brains were sectioned using a microtome (40 μM) for tyrosine hydroxylase (Bartlett et al., 2016) to verify dopamine lesion and tetrode locations.

Signal processing

Neural data was acquired at 30 kHz. For LFP analysis the data was downsampled to 500 Hz. High voltage spindles (HVS; Dejean et al., 2007) were identified and removed from LFP analysis. To detect the HVS we used a band pass filter of 8-20 Hz and the power envelop was obtained using the Hilbert function and taking the absolute value of the signal. The baseline subtracted power envelop was then convolved with a hanning kernel (1000 ms). The periods were identified as HVS when the convolved signal exceeded threshold. These periods were then removed from analysis.

Spike sorting

The single unit data was clustered using the KlustaKwik software (RRID:SCR_014480). The clusters obtained from KlustaKwik were sorted into unique spikes manually using MCLust 4.4 (David Redish, UMN) based on waveform, peak, first two principal components, and low number of spikes within the refractory period. Volume conducted noise was reduced by using common average re-referencing.

Data analysis

LFP frequencies: Wide band gamma was defined as 40 -75 Hz. Focal 50 Hz gamma was defined as 45 – 60 Hz power subtracted by the mean in adjacent bands, which were 35 – 39 Hz

and 66 – 70 Hz (**Fig. 2d**). Focal 80 Hz gamma or just the 80 Hz was defined as 78 – 90 Hz power subtracted by mean in adjacent bands, which were 68 – 72 Hz and 98 – 102 Hz. The HFO band was defined as 120 – 170 Hz.

Non-parametric Wilcoxon rank sum tests and t tests ($\alpha < .05$) were used to assess statistical significance. The spectrogram function in MATLAB was used to obtain the power in different frequency bands. All statistical analyses were conducted in MATLAB. The post injections periods used for analysis were calculated around ketamine injection times. The analysis windows were post saline, -25 to -5 min, post ketamine, 2 to 30 min, 60 min post ketamine, 60 to 80 min, and the baseline period, -35 to -50 min during saline and ketamine sessions. In L-DOPA and saline or L-DOPA and ketamine sessions, the analysis windows were post L-DOPA, -50 to -30 min, peak L-DOPA, -50 to -30 min, post ketamine or post saline, 2 to 30 min, and the baseline period, -65 to -80 min.

Neural firing rate

Spikes from each neuron were binned into 10 sec bins, and the mean firing rate was obtained. Firing rate was normalized by subtracting the baseline firing rate (15 min) from the post-injection periods. Neurons with a difference measure of greater than 0.05 Hz in any of the post-injection periods were used in subsequent analysis.

Burst firing analysis

The burst firing of a neuron was measured using a local variance measure described in Shinomoto et al., (2003) and was implemented in MATLAB. This local variance measure obtains the instantaneous spike rate and is less sensitive to firing rate fluctuations.

Spike coherence analysis

The spike coherence was obtained for each neuron and each frequency in the range of 1 to 250 Hz. To do this, the wavelet for the LFP was computed around each spike of a neuron for each frequency band specified. For a given neuron, the phase of the band passed LFP signal was determined at the time of each action potential. The phase of the filtered LFP signal was calculated using the Hilbert transform ($\text{angle}(\text{hilbert}(\text{signal}))$) in MATLAB). The Rayleigh Z measure was used to determine whether the distribution of phases for a given neuron was nonuniform (Fisher, 1995).

Experimental design

In the study, naïve ($n = 1$) and LID ($n = 1$) rats were used to investigate how ketamine affects local-field and single-unit activity. The tetrodes were implanted in M1 at surgery. At different points during the course of the experiment, the tetrodes were pushed into the striatum (**Fig. 2b**). There were three types of drug conditions (**Fig. 2a**): saline and ketamine sessions, L-DOPA and saline sessions, and L-DOPA and ketamine sessions. The naïve rat was only subjected to saline and ketamine sessions. Beta oscillations associated with the 6-OHDA hemi-lesioned parkinsonian model were seen in the lesioned but not un-lesioned hemisphere (**Fig. 2d**), which provided a between hemisphere control in the LID animal. Examples of LFP

traces are shown in **Fig 2e**, with filtered signal for 50 and 80 Hz overlaid, taken from an L-DOPA and ketamine session in the lesioned hemisphere of the LID animal.

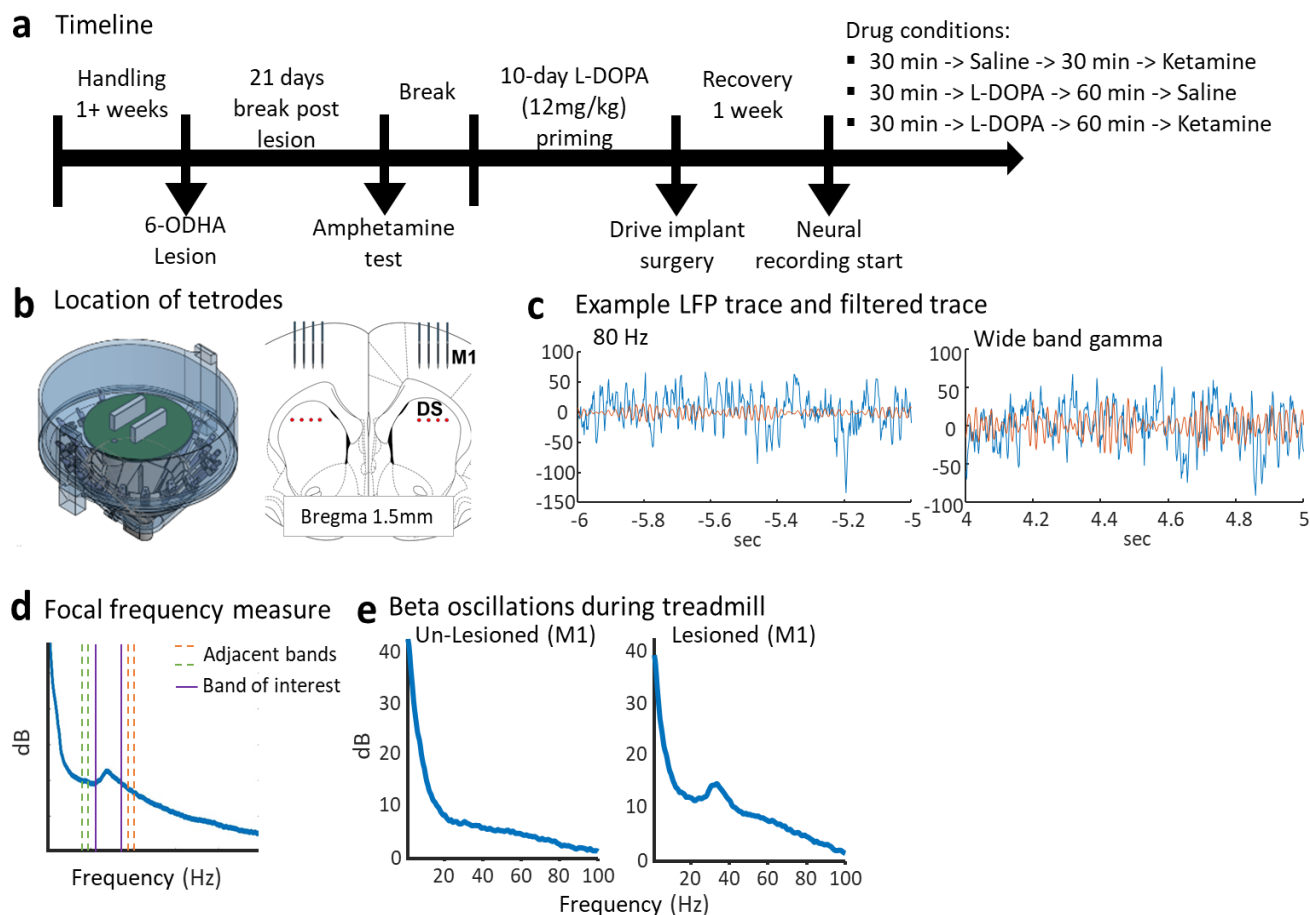


Figure 2: a) Timeline of the 6-OHDA model and the different drug conditions used in the study. b) Micro-drive used to record neural data and the locations of implants. c) Depiction of calculating the focal frequency by subtracting mean power in adjacent frequency bands. d) PSD plots during circular treadmill walking period in 6-OHDA model which shows beta oscillations in the lesioned hemisphere but not un-lesioned hemisphere of M1. e) Raw LFP data for a 1 min window in the post ketamine period (LEFT) and peak L-DOPA effect period (RIGHT) with filtered wide band gamma and 80 Hz signal overlaid, respectively.

In the naïve rat, 10 saline and ketamine sessions were used for LFP analysis for M1 and striatum. In the LID animal, there were 8 saline and ketamine session for M1 and 4 sessions for striatum. There were 8 sessions of L-DOPA and ketamine injections and 7 sessions of L-DOPA

and saline injections all in M1 used for LFP analysis. It should be stated that these are preliminary data (n = 2 rats). While the analyses below are performed across sessions due to the small sample size (n = session), analyses performed for any submitted manuscript that compares between groups (e.g., LID vs. naïve rats) will use the rat as the sample unit (n = number of rats).

Results

Ketamine-induced gamma oscillations emerge in the motor cortex of naïve and lesioned and un-lesioned hemisphere of the LID animal

The LFP activity during the saline and ketamine conditions in naïve and PD animals were analyzed to look at the oscillations produced by ketamine administration. We looked at power spectral densities and mean power during ketamine administration to assess if there were differential effects of ketamine in PD and naïve animals. We predicted that ketamine would induce wide band gamma oscillations in M1 of both the naïve and PD animals (previously reported in Ye et al., 2021). We found an increase in wideband gamma activity in M1 of the naïve rat and the lesioned and un-lesioned hemisphere of the PD rat. Power spectral density (PSD) plots after ketamine injection (2-30 min) displayed activity in the wide-band gamma range in the naïve rat, and lesioned and un-lesioned hemisphere of the PD rat (**Fig. 3b**). The spectral activity in the gamma band was then quantified around saline and ketamine injections after baseline normalization (**Fig. 3b**). There were no significant differences between the naïve and PD rats for wide band gamma power (Wilcox rank sum test, $p > .05$). The movement speed

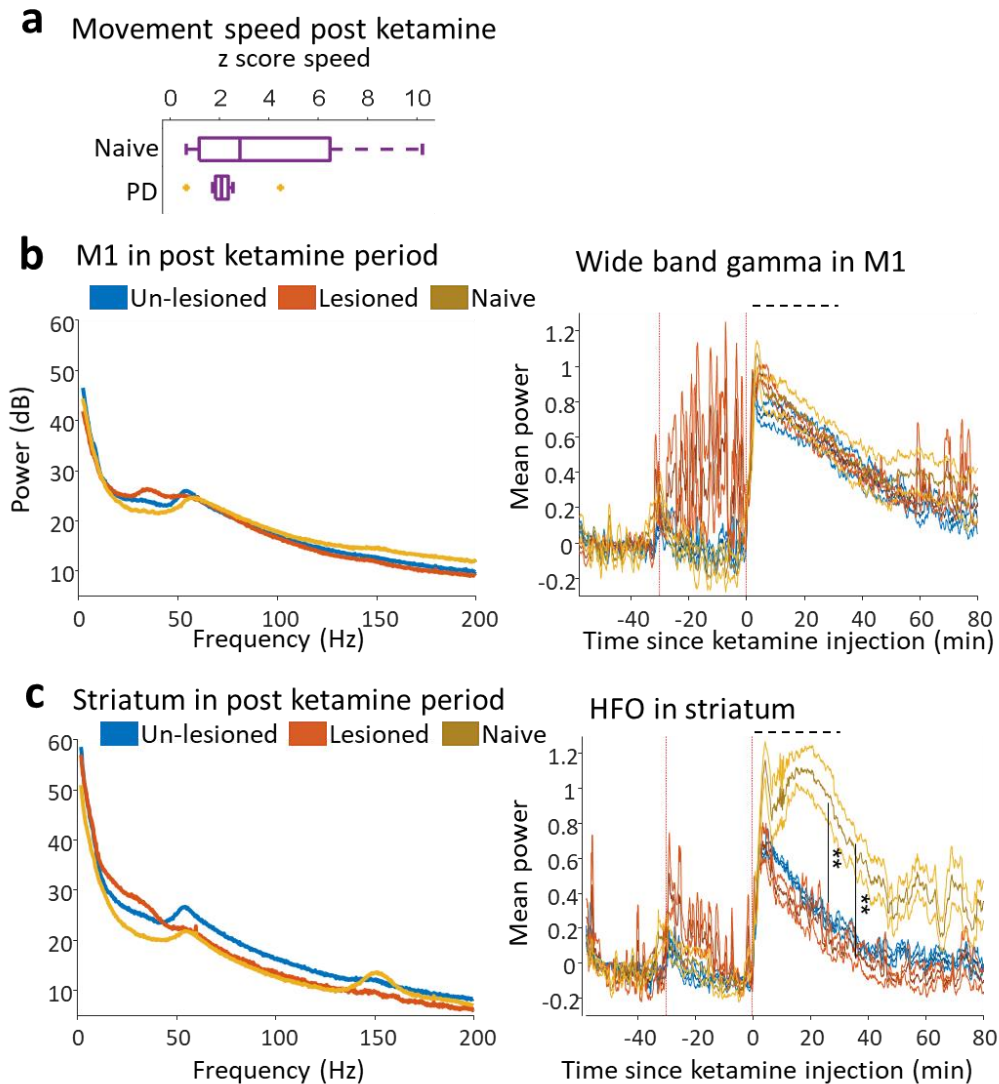


Figure 3: Differential effects of ketamine on naïve and PD rats. a) Baseline normalized movement speed in the 2-30 min post ketamine period across saline and ketamine sessions in naïve ($n = 10$ sessions) and PD ($n = 8$ sessions) rats with no significant differences. b) LEFT: PSD plot showing the 2-30 min post ketamine across sessions in M1 naïve and lesioned and un-lesioned hemisphere of PD rat. RIGHT: Mean power across sessions around saline and ketamine injections for wide band gamma in M1. The mean power differences were calculated for the post ketamine period (dashed line). The increased activity seen in the -30 to 0 min period in the lesioned hemisphere is due to high voltage spindles. c) LEFT: PSD plot showing the 2-30 min post ketamine across sessions in striatum. RIGHT: Mean power in the HFO range across sessions seen in the striatum. Statistics were done for the period shown in the dashed line. Error bars are SEM around the mean. Wilcoxon rank sum test, ** $p < .01$.

was also analyzed for the post-ketamine period in the naïve and PD rats which showed no significant differences across sessions (**Fig. 3a**).

HFOs emerge after ketamine in the striatum of the naïve but not PD rat

The spectral activity in the striatum was also quantified after ketamine in the saline and ketamine condition. HFO activity has been shown to occur after ketamine injection in the striatum of naïve rats (Ye, et al., 2018). We wanted to look at the activity in the striatum in the PD rat to see if there were differences in HFO between lesioned and un-lesioned hemispheres (**Fig. 3c**). HFO activity was only observed in the naïve rat (**Fig. 3c**), and not in either hemisphere of the LID rat. The spectral power in HFO displayed significant differences between the naïve and PD rats (**Fig. 3c**). There was a significant difference in HFO power after ketamine between the naïve rat and the lesioned hemisphere (Wilcoxon rank sum test, $p = .002$, $d = -2.34$) and the un-lesioned hemisphere (Wilcoxon rank sum test, $p = .002$, $d = -2.68$), but no difference between the lesioned and un-lesioned hemispheres (Wilcoxon rank sum test, $p > .05$).

Ketamine disrupts LID-associated 80-Hz oscillations in the lesioned hemisphere of an LID rat and reduces dyskinetic behavior

We wanted to investigate the effect of an acute ketamine injection in reducing the neural signatures of LID. We looked at the 80-Hz oscillations in the dyskinetic rat during the L-DOPA and saline, and L-DOPA and ketamine sessions. We predicted that a single ketamine (i.p., 20 mg/kg) injection would reduce the 80-Hz oscillations and reduce the behavioral symptoms of dyskinesia as well. The 80-Hz oscillations associated with LID were seen in the lesioned

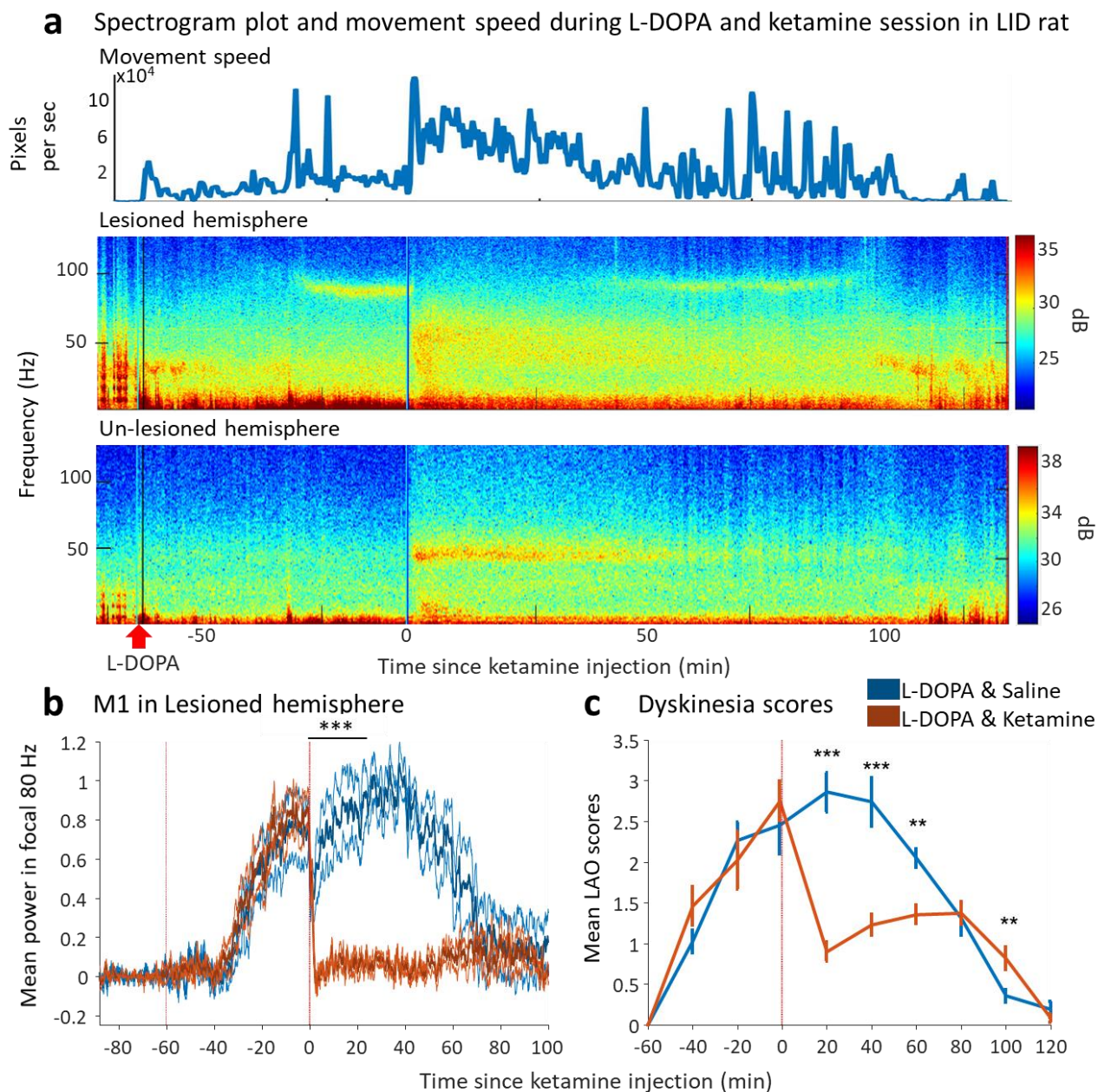


Figure 4: Ketamine disrupts 80 Hz oscillations and symptoms of LID. a) Overall movement speed in pixels per sec (TOP) from the time of L-DOPA administration to the end of one recording session. Spectrogram plots of period around L-DOPA and ketamine injections showing the power in difference frequency bands in the lesioned hemisphere (MIDDLE) and un-lesioned hemisphere (BOTTOM). b) Mean power in the focal 80 Hz gamma across sessions in M1 of lesioned hemisphere during L-DOPA and saline ($n = 7$ sessions) and L-DOPA and ketamine ($n = 8$ sessions) administration. c) The mean LAO scores of dyskinesia scored at 20 min intervals during the same L-DOPA and saline/ketamine sessions as in b). Error bars are SEM around the mean power. Wilcoxon rank sum test, *** $p < .001$, ** $p < .01$.

hemisphere of the LID animal but not in the un-lesioned hemisphere (**Fig. 4**), corroborating the LID signatures seen in previous studies using the 6-OHDA model (Halje et al., 2012; Ye et al., 2021). The spectrogram plot for a single L-DOPA and ketamine session in the LID animal displayed clear 80-Hz oscillations after L-DOPA injection in the lesioned hemisphere but not in the un-lesioned hemisphere (**Fig. 4a**). When ketamine was administered during the peak activity of L-DOPA and dyskinesia, the 80 Hz oscillations in the lesioned hemisphere were disrupted and were replaced by wide band gamma activity. In the un-lesioned hemisphere, ketamine administration elicited a narrow-band gamma activity as seen in the spectrogram plot. The spectral power of focal 80 Hz was quantified in the lesioned and un-lesioned hemisphere (**Fig. 4b**). There was a significant decrease in the power of focal 80 Hz after ketamine injection compared to saline control in the lesioned hemisphere across sessions (Wilcoxon rank sum test, $p < .001$, $d = -2.80$). In addition to changes in spectral activity in the LID animal, the dyskinetic movements were also reduced after ketamine administration (**Fig. 4c**). The LAO AIMS scores across sessions were significantly reduced for almost 60 min post ketamine injection compared to saline control (Wilcoxon rank sum test, $p < .01$).

Ketamine increases wide band gamma power in the lesioned hemisphere of the LID rat

The ketamine induced gamma oscillations were examined next. We hypothesized that the circuits generating the 80 Hz oscillations and the ketamine gamma oscillations were distinct. Thus, we analyzed the gamma activity induced by ketamine in the LID rat during the L-DOPA and ketamine sessions to analyze if there were differences in the dopamine-depleted and

the intact hemispheres. We found differences in the wide band gamma and focal 50 Hz gamma power between the lesioned and un-lesioned hemispheres (**Fig. 5**). In the lesioned hemisphere, there was a significant difference between wide band and focal gamma power post ketamine injection across sessions (Wilcoxon rank sum test, $p < .001$, $d = 3.31$). In the un-lesioned hemisphere, there was also a significant difference between wide band and focal gamma power post ketamine (Wilcoxon rank sum test, $p = .015$, $d = 1.76$); however, the effect size was smaller than observed in the lesioned hemisphere. This increase in wide band activity, but not focal gamma power, in the lesioned hemisphere is not seen as prominently in the saline and ketamine sessions (**Fig. 5b**), which may indicate a specific ketamine action during L-DOPA presence in the dopamine-depleted lesioned hemisphere.

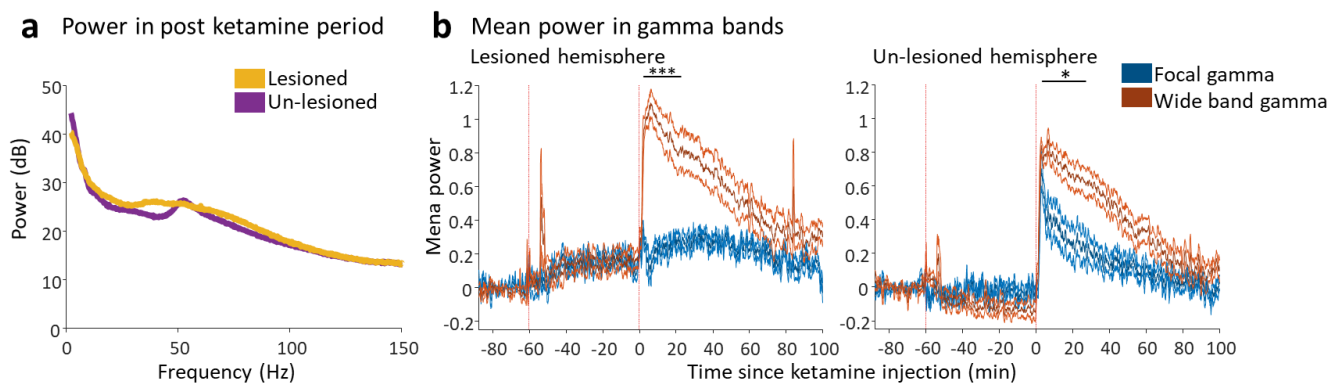


Figure 5: Wide band and focal gamma differences in LID. a) PSD plot of the 2-30 min period post ketamine injection in the lesioned and un-lesioned hemisphere. b) Mean power in the wide band and focal 50 Hz gamma during the saline (first dashed line) and ketamine (second dashed line) injections in the lesioned hemisphere (LEFT) and un-lesioned hemisphere (RIGHT). There was a significant difference between the two gamma bands in the 2-30 min period post ketamine administration. The error bars are SEM around the mean power. Wilcoxon rank sum test, *** $p < .001$, * $p < .05$.

Ketamine increases neural firing

We next looked at the neural firing rates during ketamine administration in M1 neurons of both naïve and LID rats. We restricted our analysis of the striatum neurons to only the naïve rat as we had a low neuron count of striatum neurons in the LID animal. A total of 208 neurons in M1 and 32 neurons in striatum were recorded in the naïve rat. In the LID animal we recorded from 102 neurons in the lesioned hemisphere and 206 neurons in the un-lesioned hemisphere of M1 across all conditions. Neurons that did not show any activity during baseline or post injection periods were excluded from the analysis. The time windows for analysis for saline and ketamine sessions were -25 to -5 min (time since ketamine injection) post saline, 2 to 30 min post ketamine, and 60 to 80 min as the 60 min post ketamine period.

M1 and striatum neurons increase firing post ketamine in the naïve rat. We hypothesized that ketamine's antagonistic effects on the NMDAR of PV interneurons would lead to a disinhibition of pyramidal neurons and increase neural firing. Ketamine has been shown to increase overall firing in the cortex (Guyon et al., 2021). We looked at all M1 and striatum neurons to see if ketamine induced increased firing in these neurons. The firing rate changes before and after ketamine were quantified using a difference score of the firing rate by subtracting the mean firing rate in the post saline, post ketamine, and 60 min post ketamine periods with the baseline period. We looked at the proportion of neurons that increased, decreased, or did not modulate after ketamine injection. The neurons were said to have increased in firing if the changes in firing rate from baseline firing rate was greater than .5 Hz

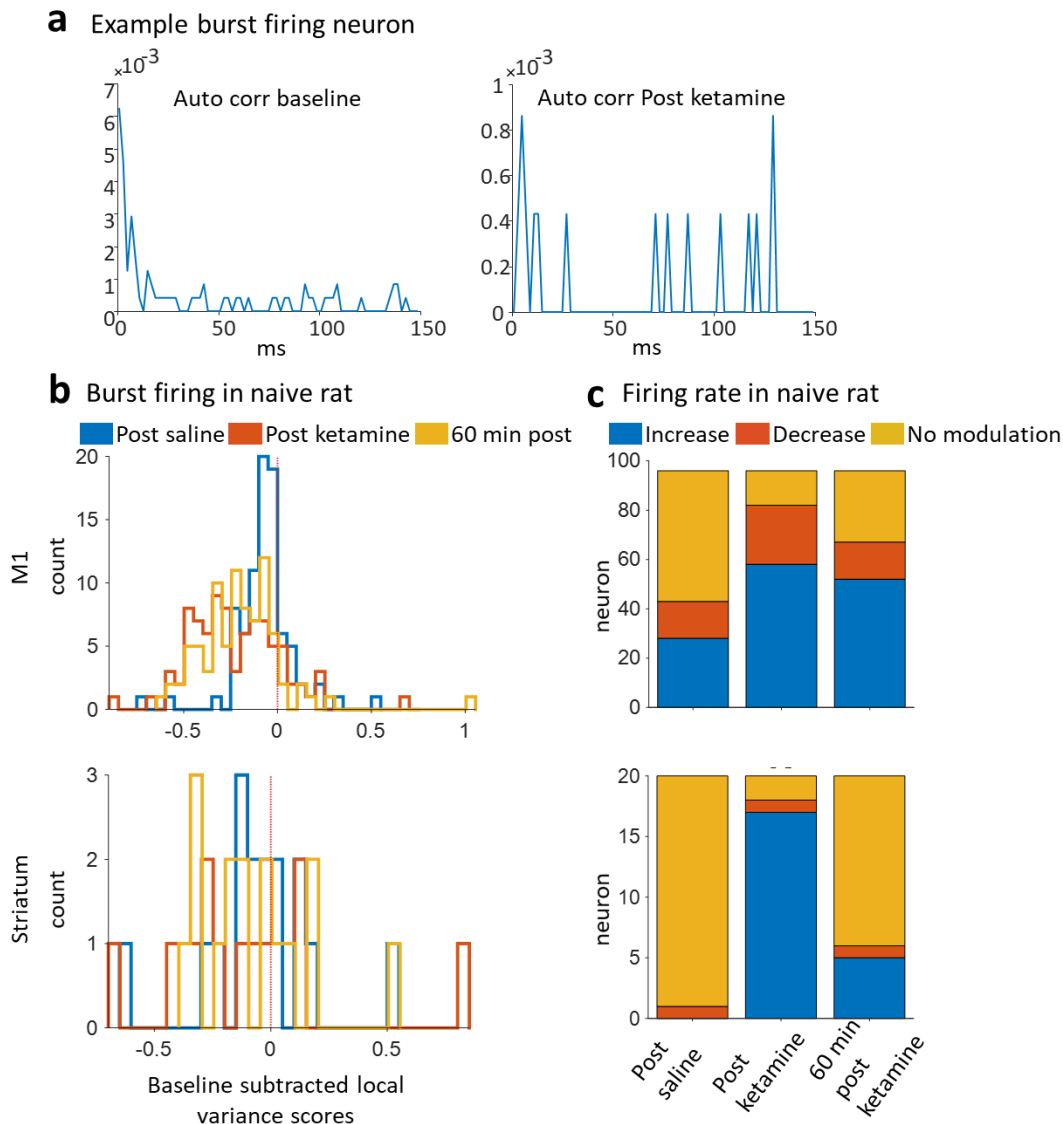


Figure 6: a) Auto correlation plots for a burst firing neuron from the naïve rat during the baseline and post ketamine period. The peak in the auto corr during the < 5 ms period is indicative of a burst firing pattern, which is not seen during the post ketamine period. b) Histogram showing difference in local variance scores for neurons in M1 (TOP) and Striatum (RIGHT) in naïve rat during post saline, post ketamine and 60 min post ketamine periods. There was significant reduction in local variance scores in all periods in M1 (t test, $p < .001$), but no significant differences in the striatum. c) Bar graphs showing proportion of neurons that increased, decreased or non-modulators in the three post injection periods in M1 (TOP) and striatum (BOTTOM). The chi square test of homogeneity showed significant changes in both M1 and striatum of naïve rat, where more neurons increased their firing immediately post ketamine in both M1 and striatum. In the 60 min post ketamine, more neurons in M1 increased firing but this effect was not seen in the striatum.

and decreased if less than $-.5$ Hz. Neurons were said to have no modulation if the difference score fell in between $-.5$ and $.5$ Hz. A chi-square test of homogeneity was used to determine if the modulation of neurons were different from baseline in the three periods of interest (**Fig. 6c**).

In M1 of the naïve rat, the proportion of neuron modulation were significant, $X^2(4, N = 288) = 38.14, p < .001$. In the post saline period, there was a significant increase in the number of non-modulators and a reduced number of neurons that decreased firing; there was no difference in the number of neurons that increased firing rate compared to baseline. Immediately after ketamine injection, there was a significant number of neurons that increased their firing and decreased in the number of non-modulators; there was no difference in the number of neurons than decreased in firing. In the 60 min post ketamine injection period, the period after ketamine's half-life effects, there was still a significant number of neurons with increased firing rate, but there was no significant number of decreased firing or non-modulation neurons. Thus, in M1 of the naïve rat, ketamine increased firing rate and the effect of ketamine on firing rate persisted for more than 60 min post injection.

In the striatum, the chi-square test of homogeneity showed a significant difference in firing rate, $X^2(4, N = 69) = 30.37, p < .001$ (**Fig. 6c**). The number of non-modulators were higher in the post saline period and significantly fewer neurons decreased or increased their firing rate in this period. In the period immediately after ketamine injection there was a significant number of neurons that increased firing and the number of non-modulators significantly

decreased post ketamine. In the 60 min post ketamine injection period the effect of ketamine was reversed, there was a decrease in the number of neurons that increased their firing rate while there was a significant increase in the number of non-modulators in this period. Thus,

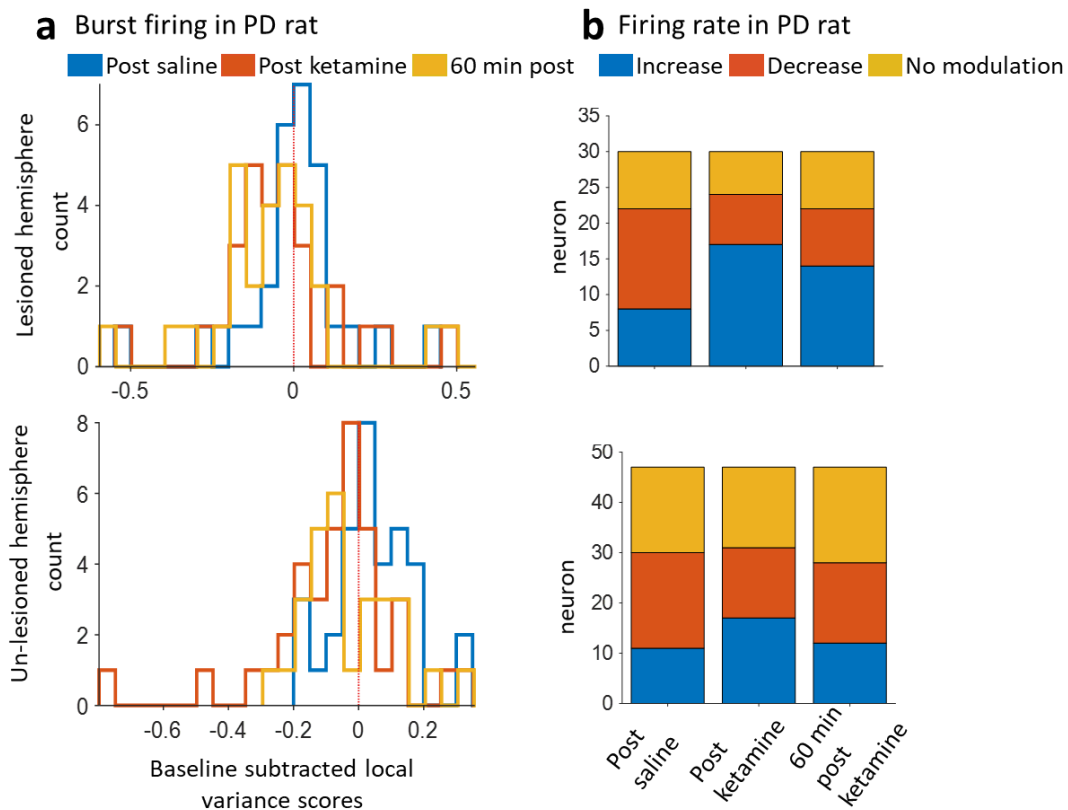


Figure 7: a) Histogram showing difference in local variance scores for neurons in lesioned (TOP) and un-lesioned (BOTTOM) hemispheres of PD rat during post saline, post ketamine and 60 min post ketamine periods. There was significant reduction in local variance scores for neurons post ketamine injection in the un-lesioned hemisphere, and no other significant differences in any other periods or the lesioned hemisphere. b) Bar graphs showing proportion of neurons that increased, decreased or non-modulators in the three post injection periods in the lesioned (TOP) and un-lesioned (BOTTOM) hemispheres. The chi square test of homogeneity showed no significant changes in neuron count in the three periods in either hemisphere.

ketamine increased neural firing in both M1 and striatum of the naïve rat, but ketamine's effects lasted for a shorter period in the striatum than in M1.

No difference in neural firing in PD model. In the saline and ketamine sessions, previously described difference measures of firing rate were calculated for post saline, post ketamine, and 60 min post ketamine periods (**Fig. 7b**). In M1 of the lesioned hemisphere, the chi-square test for homogeneity showed no significant differences in firing rate $\chi^2 (4, N = 90) = 6.59, p > .05$. There was no significance in the un-lesioned hemisphere either, $\chi^2 (4, N = 141) = 2.59, p > .05$.

No difference in neural firing in LID model. In L-DOPA and ketamine sessions, the difference measure in the dyskinetic animal was obtained as previously described for post L-DOPA, peak L-DOPA, and post ketamine periods (**Fig. 8b**). The chi-square homogeneity test showed no significance in the lesioned, $\chi^2 (4, N = 93) = 6.08, p > .05$, or un-lesioned hemisphere, $\chi^2 (4, N = 201) = 6.8, p > .05$.

Ketamine reduces burst firing

We looked at the burst firing in neurons during ketamine and L-DOPA administrations. We predicted that L-DOPA administration would lead to an increase in burst firing and ketamine would decrease burst firing. The local variance scores were obtained for each neuron as a burst firing metric (see Methods). The local variance scores were baseline normalized by subtracting the baseline variance from the three post injection periods. An example of a burst firing neuron recorded from a naïve rat, with a local variance score of 1.3 during baseline, is

shown in **Fig 6a**. In the naïve rat ketamine significantly reduced burst firing in M1 neurons (**Fig. 6**). A histogram plot shows the local variance measures of all neurons in the naïve rat in M1 and

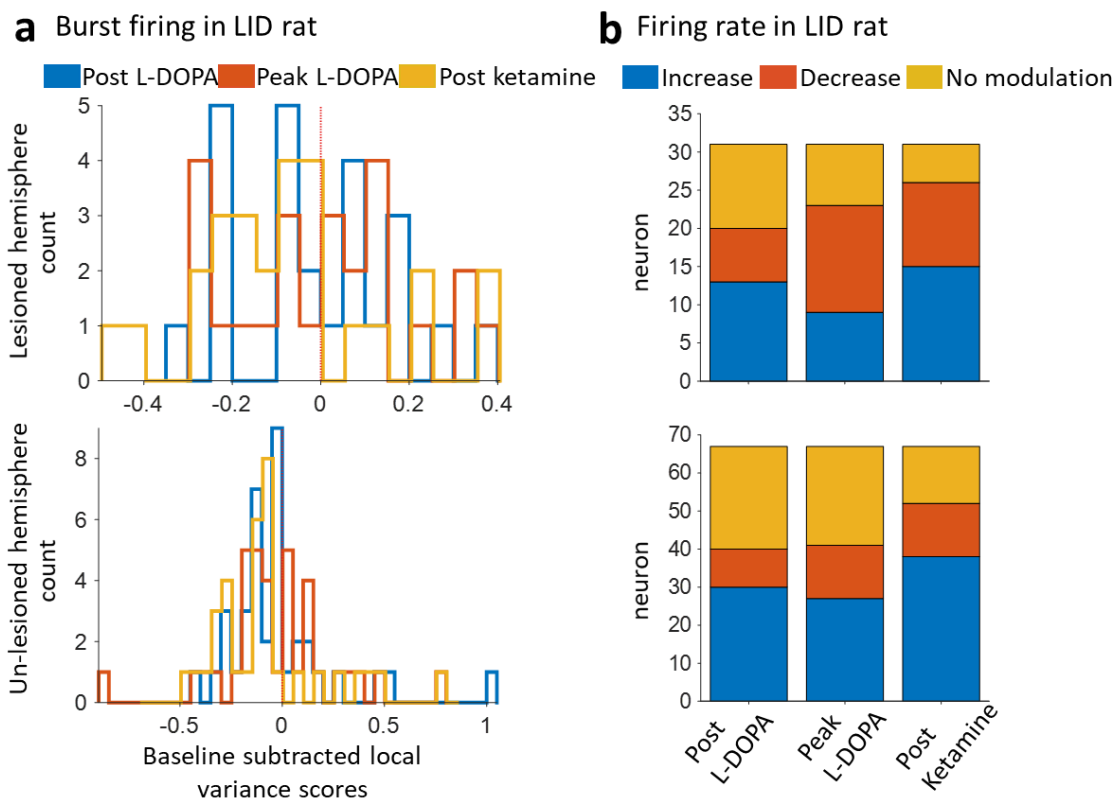


Figure 8: a) Histogram showing difference in local variance scores for neurons in lesioned (TOP) and un-lesioned (BOTTOM) hemispheres of LID rat during post L-DOPA, peak L-DOPA, and post ketamine periods. There were no significant changes in the burst measure in any periods in both hemispheres. b) Bar graphs showing neurons that increased, decreased or non-modulators in the three post injection periods in the lesioned (TOP) and un-lesioned (BOTTOM) hemispheres. The chi square test of homogeneity showed no significant changes in the number of neurons that changed their firing rate in either hemisphere.

striatum (**Fig. 6b**). The local variance measures were analyzed using a one-sample t test for the post saline, post ketamine, and 60 min post ketamine periods. We found a significant reduction in the neurons local variance scores in the post saline (t test, $p < .001$; Cohen's d , $d = -.41$), post

ketamine (t test, $p < .001$; Cohen's d , $d = -.92$), and in the 60 min post ketamine period (t test, $p < .001$; Cohen's d , $d = -.89$); however, the effect sizes of period immediately after ketamine injection and 60 min post ketamine were higher than the post saline period. In the striatum, there were no significant difference in local variance scores relative to baseline in the post saline (t test, $p > .05$), post ketamine (t test, $p > .05$), and 60 min post ketamine (t test, $p > .05$) periods.

In the PD model during the saline and ketamine sessions, there were significant differences in the un-lesioned hemisphere but not in the lesioned hemisphere (**Fig. 7a**). There was a significant reduction in burst firing immediately after ketamine injection (t test, $p = .029$; Cohen's d , $d = -.37$) in the un-lesioned hemisphere, but there were no significant differences in the post saline (t test, $p > .05$) or 60 min post ketamine (t test, $p > .05$) periods. In the lesioned hemisphere there were no significant differences in the post saline (t-test, $p > .05$), post ketamine (t test, $p > .05$) or 60 min post ketamine periods (t test, $p > .05$). During dyskinesia in the LID animal in the L-DOPA and ketamine sessions, there were no significant changes in the local variance measures relative to baseline in the lesioned or un-lesioned hemisphere (**Fig. 8a**).

Spike coherence in neurons during L-DOPA and ketamine administration in LID animal

We investigated the spike phase locking of M1 neurons to 80 Hz oscillations. We predicted to find a subset of M1 neurons in the lesioned hemisphere would phase lock to the 80 Hz oscillations. We looked at the spike coherence to phase for every frequency from 1 to 250 Hz in M1 neurons during baseline, peak L-DOPA, post ketamine, and 60 min post ketamine

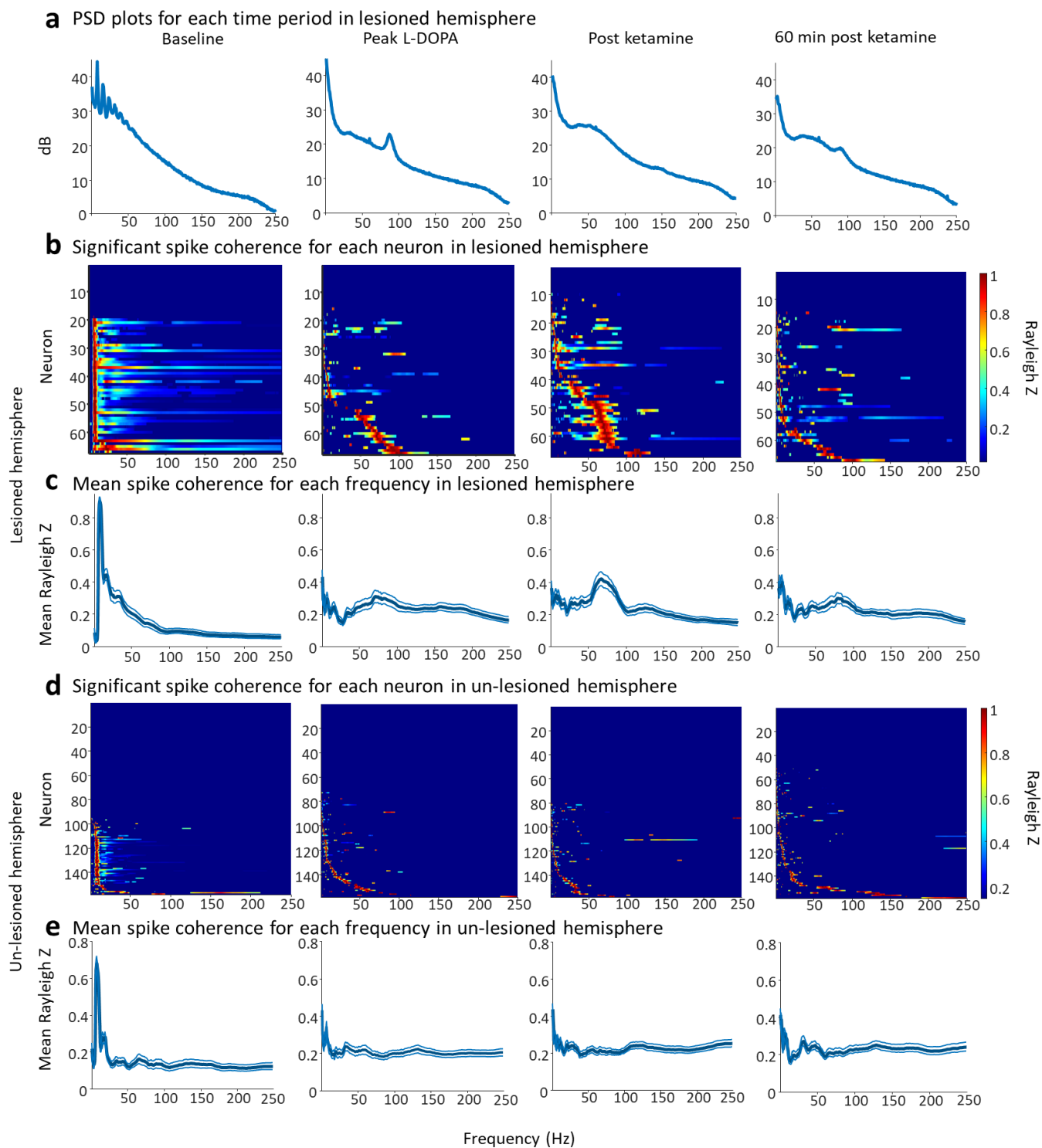


Figure 9: Spike coherence in LID rat. a) PSD plots for each time window analyzed in L-DOPA and ketamine sessions ($n = 6$ sessions). b) Significant spike coherence of all neurons in the lesioned across sessions to different frequencies (1:250 Hz). The non-significant Rayleigh Z scores ($p > .05$) appear as zero in this figure for visualization. The color scale of Rayleigh Z scores was limited to the range from 0 to 1. c) Mean Rayleigh Z scores across lesioned hemisphere neurons. d) Same as in (b) but for un-lesioned hemisphere neurons. e) Same as in (c) but for un-lesioned hemisphere neurons. The error bars are SEM.

periods for LID animal ($n = 6$ LDOPA and ketamine sessions). However, since there were no 80 Hz oscillations in the un-lesioned hemisphere (**Fig. 4a**), we analyzed spike coherence of neurons in lesioned and un-lesioned hemispheres to the lesioned hemisphere oscillations. A total of 67

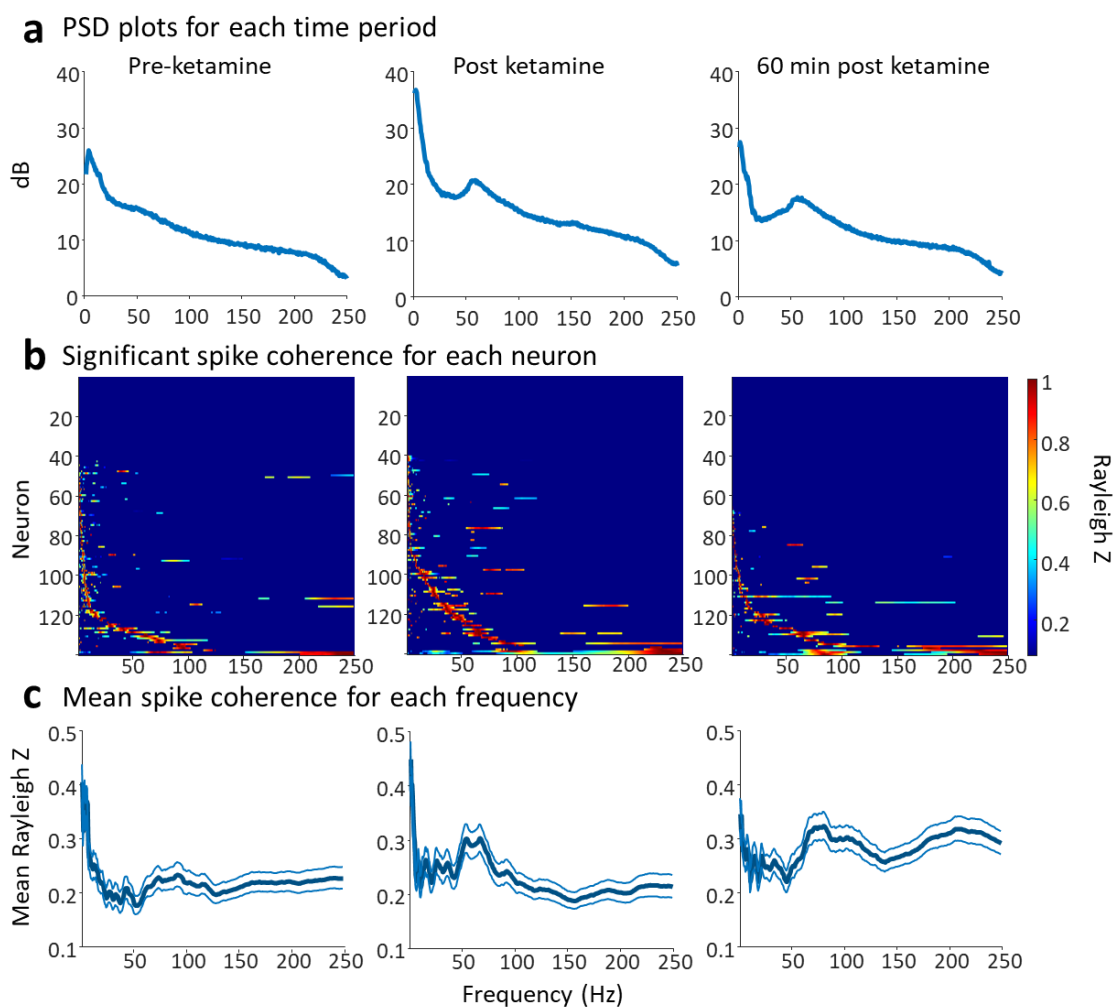


Figure 10: Spike coherence in naïve rat. a) PSD plots for each time window analyzed in saline and ketamine sessions ($n = 6$ sessions). b) Significant spike coherence of all neurons across sessions to different frequencies (1:250 Hz). The non-significant Rayleigh Z scores ($p > .05$) appear as zero in this figure for visualization. The Rayleigh Z scores were also normalized to range from 0 to 1. c) Mean Rayleigh Z scores across all neurons. The error bars are SEM.

neurons in the lesioned hemisphere, and 158 neurons in the un-lesioned hemisphere were used in this analysis. The Rayleigh Z scores were obtained for each neuron in each frequency (see Methods for details) and the significant z scores are shown in **Fig 9** for lesioned and un-lesioned hemispheres of LID rat. The PSD plots show the oscillations during the periods of analysis (**Fig. 9a**).

We compared the mean Rayleigh Z scores for each neuron in the two hemispheres for the 80 Hz range (74-94 Hz; **Fig. 12a**). The within subjects Kruskal-Wallis test for the lesioned hemisphere neurons revealed a significant difference between the time windows for spike coherence to 80 Hz ($H(3) = 42.22, p < .001$). There was significant increase in all three post injection periods compared to baseline as shown by the pairwise comparison analysis ($p < .001$), but there were no differences between the spike coherence to 80 Hz in the post L-DOPA, post ketamine and 60 min post ketamine periods ($p > .05$). The post ketamine period does not show 80 Hz oscillations in the lesioned hemisphere (**Fig. 9a**); however, it was interesting to find no differences between the peak L-DOPA and post ketamine periods. We predicted to see a reduction in spike coherence to 80 Hz in the post ketamine period but surprisingly there seemed to be an increase (**Fig. 9c**); however, this was not significant. The within subjects Kruskal-Wallis test for un-lesioned hemisphere for spike coherence to 80 Hz also revealed a significant difference between the time windows ($H(3) = 27.21, p < .001$). The pairwise comparisons revealed a significant increase in the peak L-DOPA period ($p = .003$), post ketamine period ($p < .001$), and the 60 min post ketamine period ($p < .001$) compared to baseline. The

baseline periods consisted of powerful HVS oscillations (**Fig. 9b&d**) which might explain the stark difference between baseline and post injection periods.

Spike coherence in neurons during ketamine administration in naïve animal

In the naïve animal we looked at the spike coherence to the gamma activity induced by ketamine across saline and ketamine sessions ($n = 6$ sessions). We hypothesized that there would be neurons that phase lock to gamma. In the naïve rat, 140 M1 neurons were used for analysis. The pre ketamine, post ketamine, and 60 min post ketamine periods were analyzed with the same spike coherence as used in LID animal. The significant Rayleigh Z scores for the 250 frequencies are shown in **Fig 10**, along with the means and PSD plots for each time window

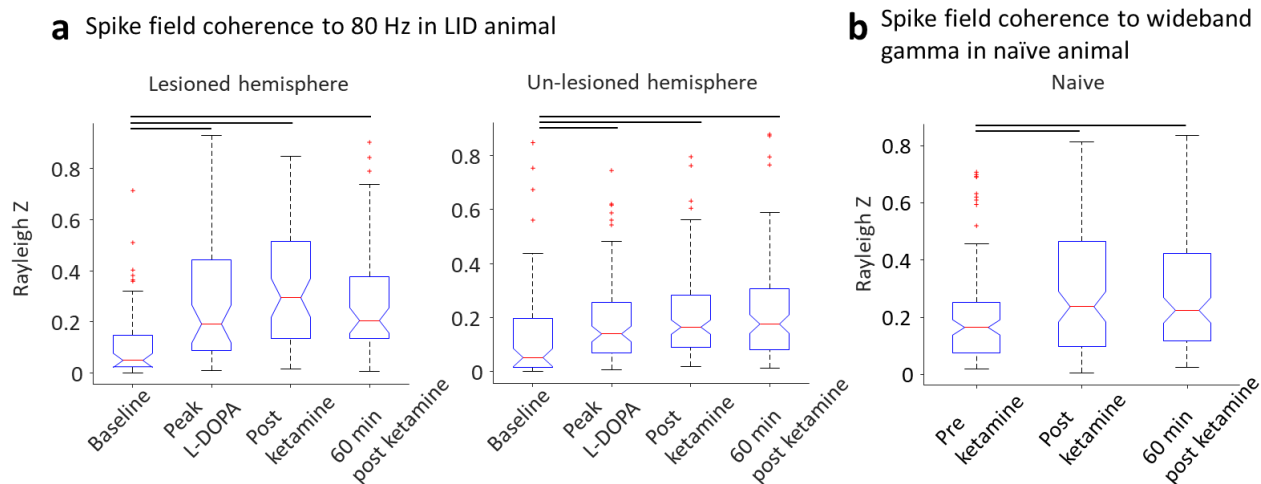


Figure 11: Box plots of mean Rayleigh Z scores for neurons in Fig. 9 and 10. a) Spike coherence to 80 Hz gamma in the lesioned (LEFT) and un-lesioned (RIGHT) hemispheres for the time periods shown in Figure 9. The horizontal lines represent significant differences ($p < .01$) between groups obtained from the pairwise comparisons after the Kruskal-Wallis test. b) Spike coherence to the wide band gamma in the naïve rat for the time periods shown in Figure 10. The horizontal lines represent significant differences ($p < .05$) between groups obtained from the pairwise comparisons after the Kruskal-Wallis test.

analyzed. We compared the mean Rayleigh Z scores in wide band gamma range (45-75 Hz) for each neuron in each time period (**Fig. 12b**). The within subjects Kruskal-Wallis test showed significant differences between the groups ($H(2) = 10.11, p = .006$). The pairwise comparison revealed a significant increase in spike coherence to wide band gamma in the two post ketamine periods ($p < .05$) compared to the pre ketamine period.

Discussion

Although dyskinesias are the most debilitating side effects of L-DOPA, the single unit and systems level nuances are less understood in LID. Here we investigated both the oscillatory signatures and single unit activity in an LID animal and explore the ability of acute ketamine administration in reducing LID. We found that ketamine disrupts the 80 Hz oscillations in the LID animal and reduces the behavioral symptoms of LID (**Fig. 4**). Ketamine induces its own wide band gamma oscillations that replace the 80 Hz in the LID animal. We found wide band (45-75 Hz) and focal band (45-60 Hz) gamma differences in the lesioned and un-lesioned hemispheres, where the lesioned hemisphere appeared to have wider gamma band activity post ketamine injection (**Fig. 5**). The neurons increased their firing post ketamine in M1 and striatum of the naïve rat (**Fig. 6**). The burst firing was reduced in M1 neurons of naïve rat and the un-lesioned hemisphere post ketamine administration (**Figs. 6,7**). Surprisingly, ketamine did not change the spike coherence to the 80 Hz oscillations in the lesioned hemisphere even in the absence of 80 Hz activity (**Figs. 9,11**).

Ketamine induced oscillations in LID and naïve animals

We found that ketamine disrupts 80 Hz oscillations associated with LID as measured in the lesioned hemisphere of the LID rat (**Fig. 4**). Ketamine also reduced dyskinetic movements in this animal (**Fig. 4**). This finding supports previous reports of ketamine's ability to reduce LID oscillations and symptoms (Bartlett et al., 2016; Ye et al., 2021). Ketamine also induced wideband gamma activity during the dyskinetic period in the LID rat. There were differences in the power of the wideband and focal gamma in the lesioned and un-lesioned hemispheres. We found a greater difference in the dopamine-depleted hemisphere for the wide band to focal gamma power during the dyskinetic state. Qualitatively, gamma power shown in the PSD plots of the lesioned hemisphere during the PD state (**Fig. 3b**) had more focal gamma band power compared to the dyskinetic hemisphere (**Fig. 5a**). In future analyses, we will investigate this difference in gamma power by directly comparing PD and LID states to see if the wideband and focal gamma differences are unique to the dyskinetic state or more specifically the presence of L-DOPA.

In the healthy control, ketamine induced wideband gamma activity in M1 and HFO activity in the striatum (**Fig. 3**). HFOs, however, were not seen in the striatum of the 6-OHDA model in either the lesioned or un-lesioned hemispheres. HFO activity post ketamine administration has been reported previously in the dorsomedial and dorsolateral striatum using the 6-OHDA model (Ye et al., 2021). HFOs in the motor cortex have also been observed following ketamine administration in naïve rats (Cordon et al., 2015). It was interesting to not

observe any HFO activity in our PD model but note that this was data from one rat. If this absence of HFOs in the striatum persists across animals in our future analysis it would point to some intriguing nuances in the PD model.

Increased firing and reduced burst activity in neurons after ketamine administration

Individual neuron activity in the naïve rat increased in the period immediately following ketamine injection in both M1 and dorsal striatum. Firing rate was analyzed in the 60 min post ketamine period as well. During this period, the behavioral effects of ketamine were no longer present. In M1 of the naïve rat, there was a significant increase in firing rate 60 min post ketamine, which was not observed in the dorsal striatum. This could indicate that cortical input from M1 may be driving the activity neurons in the striatum. The pyramidal cells in M1 make excitatory connections onto the medium spiny neurons (MSN) which make up most striatum neurons (Underwood & Parr-Brownlie, 2021). Thus, the increased activity in M1 due to ketamine could be driving the increase in striatal neuron activity seen in our study. Ketamine could also be directly inhibiting the PV interneurons in the striatum that disinhibit the MSNs, causing an increase in activity. However, given that the striatal neurons in the 60 min post-ketamine period did not show an increase in firing like the M1 neurons, it might be less likely that ketamine's direct effects in the striatum are as strong as the cortical input. In dopamine depleted conditions, ketamine's potential to increase activity in the striatum through cortico-striatal connections could result in some of the beneficiary effects of ketamine in LID states.

In the PD and LID states, there were no clear differences in firing rate in M1 during post ketamine or post L-DOPA injections. There have been studies that report increased neural firing in PD model in the dorsal striatum and GPe (Chen et al., 2001; Ellens & Leventhal, 2013), and some studies report a decrease in firing in M1 of PD animals (Underwood & Parr-Brownlie, 2021).

Ketamine reduced burst firing in M1 of the naïve rat and its effects were noted even after 60 min post injection. There were no significant changes in burst firing in the striatum of the naïve rat or the lesioned hemisphere, but we recorded a significant reduction of burstiness in M1 of the un-lesioned hemisphere post ketamine during PD state. We did not find any changes in burst firing patterns during the LID states in either post L-DOPA or post ketamine periods. Some studies have demonstrated increased burst firing in PD models in M1 (Goldberg et al., 2002; Pasquereau & Turner, 2010) and dorsal striatum (Chen et al., 2001). The ability to reduce burst firing could be one of the mechanisms employed by ketamine to interfere with LID oscillations which might be generated through increase burst firing of interneurons and pyramidal cells.

Spike coherence as a result of ketamine

The experiment done in Halje et al. (2012) found only a subset of M1 neurons (12% of pyramidal cells and 18% of interneurons) to be phase locked to the 80 Hz oscillations in LID animals. In our spike coherence analysis, we found 11% of neurons in the lesioned hemisphere with significant phase locking to the 80 Hz oscillations (**Fig. 9**). We initially predicted that the

effect of ketamine on the spike coherence to 80 Hz would reduce as ketamine disrupts the 80 Hz oscillations. However, ketamine did not show a significant change in spike coherence to 80 Hz compared to the peak L-DOPA period (**Fig. 11**), and instead appeared to have an increased spike coherence to that frequency range. We found increased wide band gamma activity post ketamine in the lesioned hemisphere (**Fig. 5**), and the spike coherence post ketamine could be due to this wide band gamma rather than the pathological 80 Hz oscillations.

Future directions

We will collect data from more animals (n=4 per group so n= 8) and record from more neurons to further investigate the effects of ketamine in LID and PD models. Since, this is preliminary data, the low neuron count in the PD animal could have resulted in non-significant effects of burst firing and firing rate changes. Given that ketamine has shown to have a direct effect on the NMDAR in inhibitory PV interneurons in the cortex (Carlen et al., 2012; Guyon et al., 2021; Hudson et al., 2020), we plan to classify cells into interneurons and pyramidal cells based on waveform shape and firing rate differences. This would allow us to look at differential effects in different cell types post ketamine administration in different disease states. We predict that in the interneurons there would be decreased burst firing and overall firing rate post ketamine administration due to NMDAR blockade. In pyramidal cells, we predict that ketamine would reduce burst firing but increase overall firing rate due to the disinhibition in these cells.

Other future investigations would include identifying discrete events in the 80 Hz, gamma, and beta oscillations. Although these oscillations appeared to be continuous, they occurred in bursts and thus we think that there might be significant phase coherence during these bursts of activity. We will also look at phase-amplitude coupling changes during ketamine administration in the discrete events identified. Further, we will explore differences in high voltage spindle oscillations between naïve and dopamine depleted animals. The high voltage spindles have a distinct spike-wave pattern occurring in a frequency range of 5 – 13 Hz (Dejean et al., 2007). These oscillations occur only when the animal is immobile and disappear immediately once in motion (Berke et al., 2004). The occurrence of high voltage spindle activity has been shown to increase during blockade of general and specific dopamine receptors (Yang et al., 2013) and in dopamine depleted rats using the 6-OHDA model (Ge et al., 2012), indicating the role of dopamine and cortical-basal ganglia networks. Spike entrainment to these oscillations have been studied in the striatum of naïve rats (Berke et al., 2004), which show differences of entrainment between the MSNs and PV interneurons of the striatum. We will look at the spike entrainment to the high voltage spindle oscillations in both M1 and striatum in the 6-OHDA model in our future analysis.

Limitations

We were limited in our capacity to explain the observations and differences in our study as data was acquired from one rat in the LID group and one rat in the naïve group. There was

also a disproportional neuron yield between the lesioned and un-lesioned hemispheres of the 6-OHDA model. There were fewer neurons recorded from the lesioned hemisphere.

Chapter 2

A novel integrated string-pulling behavior quantification system with simultaneous neural recording capability

Introduction

Motor cortex neurons

Neurons in the motor cortex and supplementary motor areas have been shown to encode for different aspects of movement, including motor planning (Economo et al., 2018; Cisek et al., 2003), target location in extrinsic space (Shen & Alexander, 1997), specific movement sequences (Brown & Teskey, 2014), etc. Intracortical micro-stimulation (ICMS) has been used to map the motor cortex areas responsible for specific movements (Brown & Teskey, 2014; Bonazzi et al., 2013). Arm, wrist, and digit movements were assessed post short and long duration ICMS, in head fixed rats. These studies found that short duration ICMS elicited simple movements, such as wrist extension or elbow flexion, and long duration ICMS elicited complex sequence movements, such as lift or grasp actions (Brown & Teskey, 2014; Bonazzi et al., 2013). Ensemble level activity have been explored to better answer the function of motor cortex neurons using dimensionality reduction methods (Lara et al., 2018; Shenoy et al., 2013), which account for the more abstract functions of the motor cortex neurons in producing goal directed movement. However, there is still an ongoing debate of the specific function of the motor cortex neurons. Thus, there is a need for understanding the organization of the motor cortex by

analyzing the individual and ensemble activity during complex segmented movements with sub second precision.

Complex motor tasks

The kinematics of goal-oriented tasks have been studied in complex tasks, such as the single pellet skilled reaching task in rats (Brown & Teskey, 2014; Whishaw et al., 1991; Whishaw, 1996) and staircase reaching task (Baird et al., 2001). The skilled reaching task offered fine motor movement analysis, such as wrist pronation, digit flexion and body position, in rats and mice that were trained to reach for a small pellet through a narrow door using a single paw. The differences in control and motor cortex lesioned rats were examined showing specific deficits in the ability to pronate and flex the wrist to reach and grab the pellets (Whishaw, 1996). However, these tasks require extensive training and although complex they do not allow un-restricted movement to the animals.

String-pulling task

The string-pulling paradigm (Jacobs & Osvath, 2015) has been used in a wide array of species for different cognitive and learning assessments or for investigating motor aspects of the behavior. Traditionally, the task involves a string with a reward tied out of reach at the end of the string and the ability of the subject to use the string to get the reward is assessed. As a task it is simple to design and can be altered into several variations to fit the assessment, including string orientation (Heinrich, 1995), string length (Blackwell & Wallace, 2020), effort measurements (Porter & Hillman, 2019), testing memory of string-pulling action in humans

(Singh, 2019), etc. The task has been studied in 163 species; showing varying inter and intra individual species differences of technique and learning effects (Jacobs & Osvath, 2015).

More recently, the string-pulling behavior has been characterized into distinct segments by Blackwell et al., in mice and rats (2018a, 2018b, 2018c). The bimanual movement analysis in rodents allows for complex phase analysis of the hand over hand motion and also helps to access the body position and head position of the rodents as they are required to stand upright on their hind legs in order to pull the vertical strings. The kinematics of the string-pulling behavior have been distinguished into five segments comprising of the lift, advance, grasp, pull and push sequences of hand over hand motion (Blackwell et al., 2018a, 2018b). In addition, the effect of sensorimotor lesion was compared to intact rats to access differences of the reach and withdraw phases in the string-pulling task (Blackwell et al., 2018c). The group used a MATLAB toolbox to analyze the videos using automatic color-based or manual color recognition image segmentation for pulling out the kinematics in the string-pulling (Inayat et al., 2020). Although the string-pulling task has been used widely and quantified behaviorally, the neural correlates of motor neurons during the task has never been studied.

In this report, we present an integrated “infinite string-pulling system” with the ability to record and sync to neural data. The infinite loop allowed for continuous behavior recording without having to replace strings and offered greater string lengths per trial. The motion tracking was done using DeepLabCut (Mathis et al., 2018). Video acquisition and neural recording were done simultaneous to the behavior.

Methods

Animals

Male Sprague-Dawley rat (n = 1; 280-320 g at arrival, Envigo, Indianapolis, IN, United States) were housed individually in a 12-h reverse light/dark cycle (i.e., lights off from 9AM to 9PM) room with food and water available ad libitum. All procedures were in accordance with NIH guidelines for the Care and Use of Laboratory Animals and approved IACUC protocols at the University of Arizona.

System design

Infinite pulley system and rotary encoder. The apparatus for an infinite loop was constructed using a series of pulleys around a frame of extruded aluminum bars (Zyltech Houston, Texas, United States; **Fig. 12d**). The rat pulled one end of the loop from an elevated platform in the middle of the infinite loop set up. One of the pulleys in the system was substituted with a 3D printed wheel attached to a 600-pin rotary encoder (BQLZR, Shenzhen, China) controlled by an Arduino MEGA (Arduino, Somerville, Massachusetts, United States). The length of the string pulled was obtained using the rotary encoder which was also attached to an automatic feeder that dispensed pellets based on the desired distance pulled (**Fig. 12c&d**).

Video acquisition and motion tracking. A MakoU130b camera (Allied Vision, Stadtroda, Germany) was used to acquire videos at a high frame rate (367 fps). The camera was configured with the Image Acquisition Toolbox in Matlab2019b. After collection, video information was

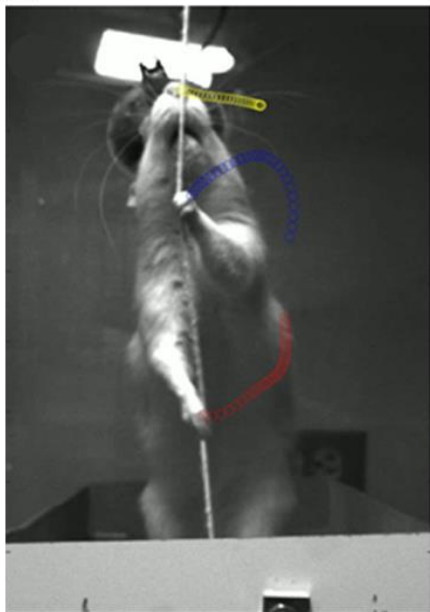
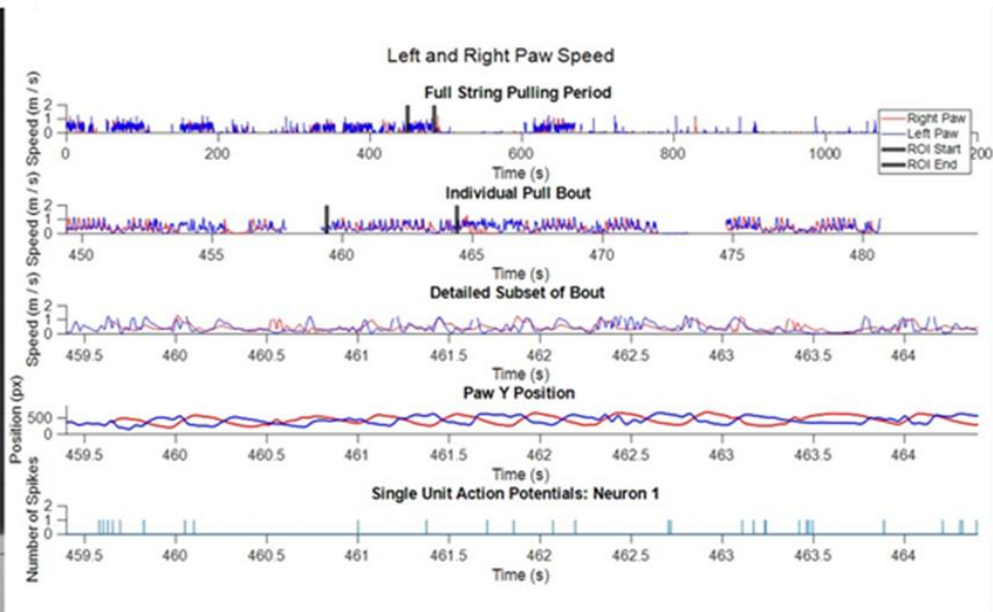
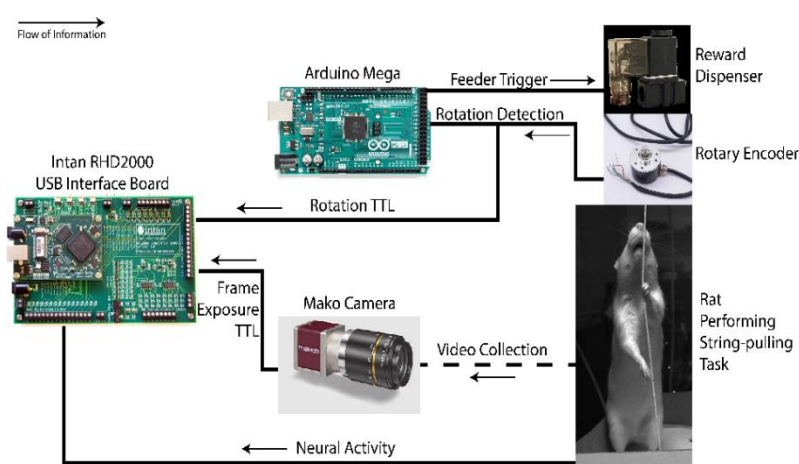
a Still image of the task**b** Synchronized kinematics, position and neural data**c** Behavioral quantification system diagram**d** Infinite loop system set up

Figure 12: System design. a) A still image of the rat performing the string-pulling task. The position data from DeepLabCut and filtered Matlab coordinates of the nose, left paw, and right paw are overlaid in yellow, blue, and red respectively. b) The speed of one session of string-pulling is shown in the first three rows, where the first row shows the full session and the next two rows shows only the bout of magnified region of interest. The fourth row shows the position data of right and left paws for the same period as in row three. The last row shows the neural activity for the period the rows three and four. This demonstrates the simultaneous and synchronized data obtained from the system. c) The system diagram showing the camera and Arduino subsystems configured to send TTL pulses to the INTAN board periodically to align neural and behavior activity d) Image of the full set up of the infinite loop system.

processed by DeepLabCut (Python) and custom Matlab code (github.com/GiaJordan/Behavior_Quantification).

For motion tracking the deconvolution neural network (DeepLabCut, Mathis et al., 2018) was first trained using 108 manually scored images (training frames) to identify the nose and paws of the rat. Each training frame was then human scored to identify the nose and paws. This information after human scoring was used by the network to improve its estimation. The network was further trained for 730,000 iterations using the labeled video frames on a 85:15 (Train:Test) split until the loss converged at 0.003. Labeled test images were used to test the accuracy of the neural network. The x and y positions of the nose and right and left paws obtained from the network was used for analysis after smoothing and interpolating for missing values.

Synchronization of neural and behavior components. Neural data was acquired using the INTAN RHD USB Interface Board. The signal from the animal was transmitted using a light-weight tether attached to the digitizing head-stage connected to the animal. The INTAN board contained 16 Digital I/O pins capable of receive Transistor-Transistor Logic (TTL) pulses from other systems.

The video camera and the rotary encoder sent TTL pulses to the INTAN board through circuits designed to process the data that was compatible with the INTAN system (**Fig. 12c**). The timestamps from the camera were aligned to the position CSV coordinates output by DeepLabCut in Matlab. This way the timestamps from the subsystems were synced to the

neural data. All recordings were conducted in a faraday cage (47 X 55 cm). The string-pulling task lasted for a period of 20-25 mins in each session.

Behavior training

The rat was food restricted to about 85% of their body weight. The rat was then habituated using 20 strings of varying length from .3 m to 1.5 m with half the string baited with cheerios and left in the arena for an hour or until the rat had pulled all the strings into the arena. Once the rat had pulled all 20 strings for two consecutive days, the rat was introduced to baited single strings of increasing lengths, starting from 1 m to 3 m. After the single strings the rat was switched to the infinite loop apparatus and trained to pull the string with manual rewards. The rat was trained to pull 4 loops consistently, where one loop around the pulleys was 2 m.

Drive implant

Once the rat was trained to pull the string consistently, the rat was prepped for surgery. The surgery was performed using isoflurane (1.5–2.0%; VetOne, Boise, ID). Dual bundle micro-drive with 16 movable tetrodes (8 tetrodes in each bundle; NeuroTek, Toronto, Ontario, Canada) were implanted in left and right primary motor cortex (center coordinates: AP = +1.5mm, ML = +2.2mm, DV > -2.5mm from bregma and brain surface) and moved into the striatum (DV < -3 mm). A skull screw over cerebellum was reference and ground. The tetrodes were moved before every unique recording session. Rats were allowed to recover for 1 week before testing.

Spike sorting

The single unit data was clustered using the KlustaKwik software (RRID:SCR_014480). The clusters obtained from KlustaKwik were sorted into unique spikes manually using MCLust 4.4 (David Redish, UMN) based on waveform, peak, first two principal components, and low number of spikes within the refractory period.

Behavior segmentation and analysis

The string-pulling behavior was segmented into reach and withdraw phases as described in Blackwell et al., using the filtered coordinates and derived velocities of each paw (2018b). Sustained positive velocity in the y axis was identified as the reach phases while sustained negative velocities were identified as the withdraw phases (**Fig. 13a&b**).

The reach and withdraw phases were further divided into segments. The reach phase was divided into lift, advance, and grasp segments (Blackwell et al., 2018b). The lift segment began at the start of upward motion and ended when the paw reached its maximum x coordinate away from the center of the body. The advance segment started at the end of the lift segment and ended at the beginning of the grasp segment. The beginning of the grasp segment is characterized by medial movement of the arm with respect to the body (**Fig. 13c**). The transition point from advance to grasp was defined as the point when the velocity in the y direction is 0.5 standard deviations less than the mean velocity from the end of lift to the end of the upward motion.

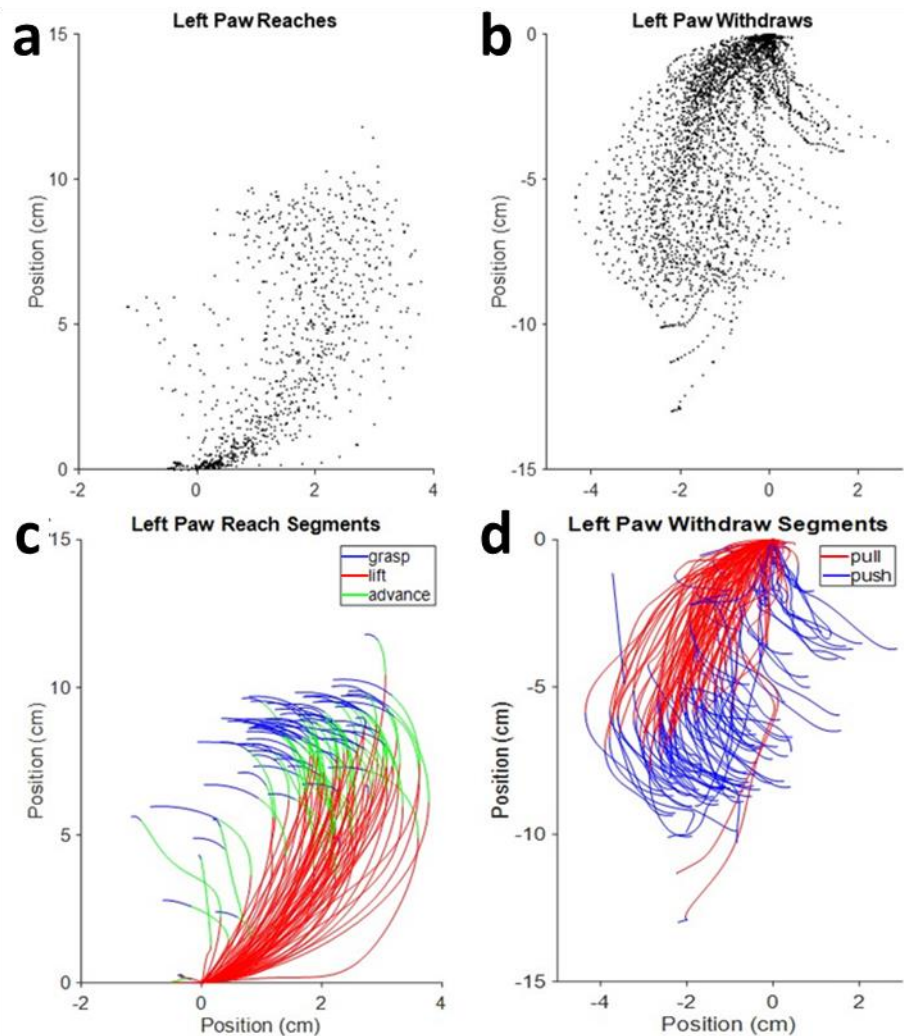


Figure 13: Behavior segmentation of the string-pulling behavior. Trajectories of the left paw during the reach phase (a) and withdraw phase (b) for one session. The segmented reach phase into lift, advance, and grasp segments for one session (c). The segmented withdraw phase into push and pull segment for one session (d).

The withdraw phase was divided into pull and push segments (Blackwell et al., 2018b).

The pull segment started with the start of the withdraw phase and the end of the pull was defined as the peak x coordinate away from the rat's center of mass. The push segment comprised of the remaining withdraw phase (**Fig. 13d**).

All post-processing, filtering, and statistical analyses were performed using Matlab2019b and Python 3.6. Non-parametric Wilcoxon rank sum tests ($\alpha < .05$) were used to assess statistical significance.

Results

Neural data and string-pulling behavior were recorded from 1 naïve rat using the integrated string-pulling system. A total 259 neurons across 10 sessions of string-pulling behavior were analyzed for this study.

Validation of motion tracking

The DeepLabCut motion tracking yielded a small error between the estimated feature positions and the manually labeled positions, which were 1.04 pixel (~ 0.027 cm) error for the training split images and a 4.33 pixel (~ 0.105 cm) error for the test images. In comparison to the paw widths (~ 35 px or ~ 0.92 cm) the detection error of the test images from the network was at an acceptable level of accuracy.

Preferential firing of neurons to paw movements

The firing of individual neurons and ensemble activity were accessed during different phases of string-pulling. The activity of neurons at paw locations during the reach and withdraw phases were analyzed to see if there was preferential firing during a particular phase. The reach and withdraw phases for all sessions and the corresponding neural spikes were identified. An example neuron is shown in **Fig 14**. This neuron preferentially fired (Wilcox ran sum test, $p <$

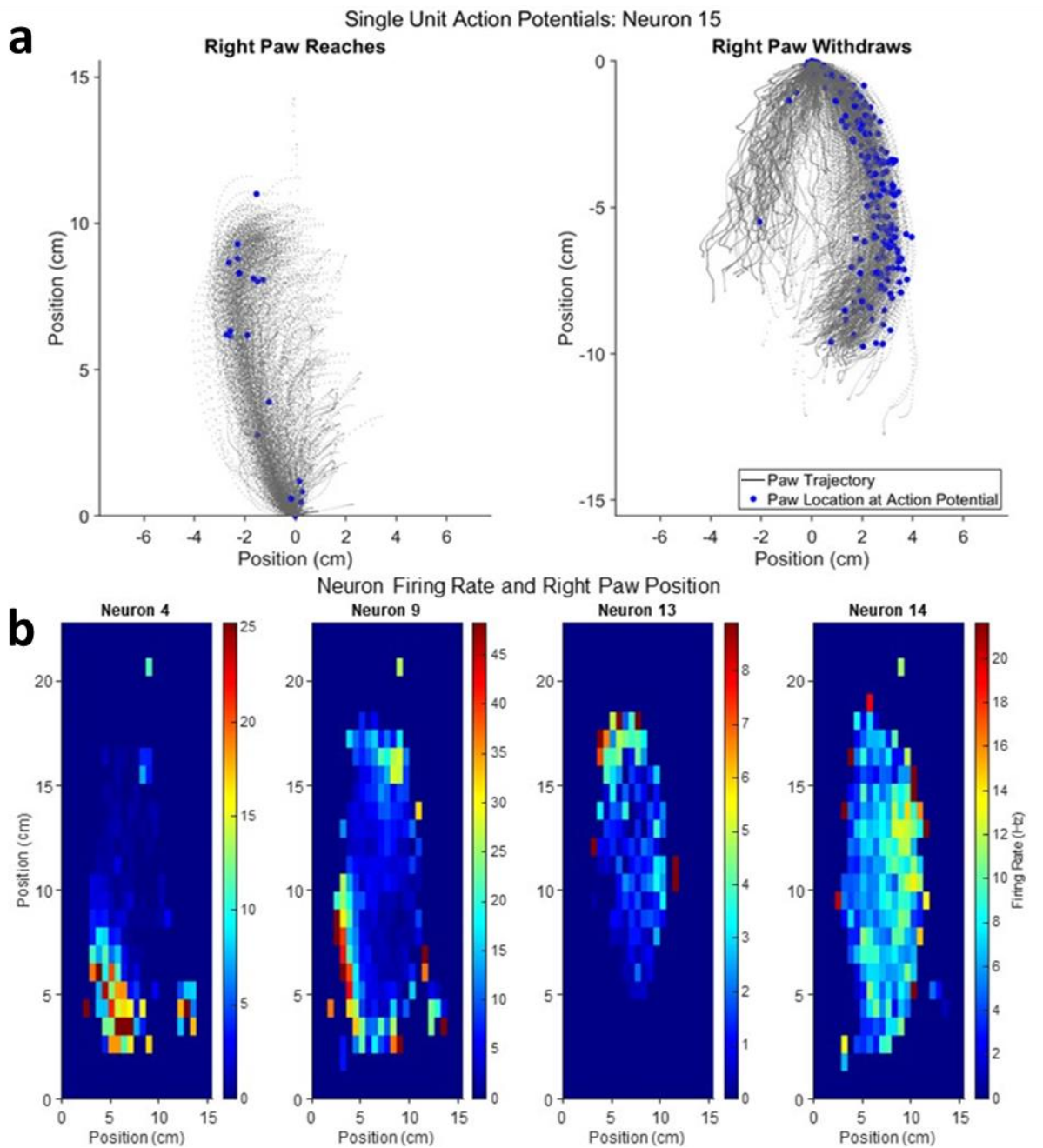


Figure 14: Preferential firing of neurons in M1 to string-pulling phases. a) Example neuron that fired more preferentially to the right paw withdraw phase of the behavior. The firing to phase preference was determined by performing a Wilcoxon rank sum test ($\alpha < .05$) on the distribution of firing rates for each phase. b) Four neurons showing preferential firing to different right paw positions during a session. The spectrogram plots show the x and y positions of the right paw and the neural firing at those paw locations, normalized for occupancy.

.05) more during the withdraw phase than the reach phase in one session. Preferential firing was further accessed by looking at all positions of a single paw during a session. Different neurons seemed to fire at different preferred locations during the task (**Fig. 14b**).

The segmentation of the behavior also allowed to look at neural firing at the onset or offset of each segment individually. An example of a neuron that showed modulation to the

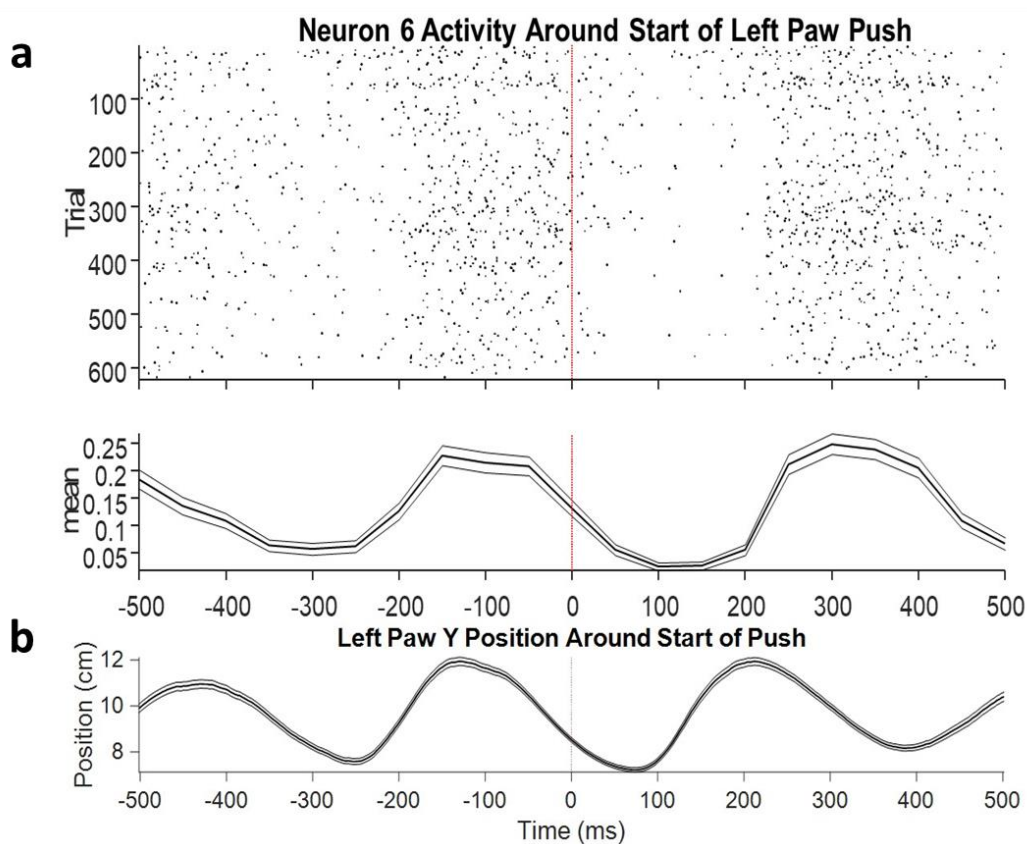


Figure 15: Peri-event histogram (PETH) and position data for the onset of push segment in the left paw. a) TOP: PETH plot showing the firing of one neuron in all trials in one session for the left paw for 500 ms before and after the onset of a push segment. BOTTOM: The firing of the same neuron averaged across all trials. b) The position in y coordinates of the left paw averaged across all trials surrounding the push segment onset. Error bars are SEM.

onset of a push segment in the left paw is shown in **Fig 15**. This modulation appeared to correlate with the position of the left paw as well (**Fig. 15b**).

Discussion

The string-pulling task offers a complex bimanual behavior that can be used to understand the kinematics and associated neural activity during this behavior. Our system demonstrates the ability to quantify this behavior at each phase and record from individual neurons at the same time. The infinite loop design offers a variety of desired lengths without having to replace strings after every trial. The addition of an automated reward system integrated with the rotary encoder also offers an automated shaping paradigm for the task. The high-resolution image acquisition and motion tracking using the DeepLabCut software yielded reliable and accurate tracking of the paws and nose. With our system, we were able to quantify some of the kinematics published previous using other software (Blackwell et al., 2018c; Inayat et al., 2020), such as total distance traveled, peak speed, average speed, elapsed time, displacement, and path circuitry on a segment-by-segment basis.

In addition, we were able to record from several neurons across 10 sessions with paw and nose positions in each session. The consistent reach and withdraw motion in the bimanual task allow for the study of the naturalistic movements and the neural correlates for these action in the motor cortex. With our system we identified some preferential firing of neurons to different segments of the behavior. This can be further studied to understand the functional organization of the motor cortex using the integrated string-pulling system.

Applications and Future directions

The string-pulling task is a versatile task that can be adopted in various ways based on the type of assessment. The infinite loop system can be modified to study different movements by altering the string orientation for example. Furthermore, it can easily be adapted as a cognitive task by introducing multiple strings to study decision making, probability learning, and reward prediction. The automatic feeder offers an easy adaptation to probability reward variations.

The task can also be used to study the effect of lesions (Blackwell et al., 2018c) and other motor deficit models to distinguish the limb differences and corresponding neural activity. We are interested in the motor and cognitive deficits involved in PD. The string-pulling system equipped with motion tracking and neural recording system can be used to study the fine motor differences in the hemi-lesioned 6-OHDA PD model. The bimanual string-pulling task is a better task than the ones used for assessment of PD currently. Thus, it can assist in pulling apart the differences in limb use and neural correlates in M1 of the dopamine-depleted hemisphere, for example. In addition, the recovery of movement in the contralateral limb with L-DOPA administration can be quantified using the paw kinematics described in our analysis.

Author Contributions

For chapter 1, A.V was involved in conception and design of the study, collected the data, and performed most of the analysis. In chapter 2, A.V contributed to the design of the study and data collection. The thesis was written by A.V.

References

- Allred, R. P., Adkins, D. A. L., Woodlee, M. T., Husbands, L. C., Maldonado, M. A., Kane, J. R., ... Jones, T. A. (2008). The Vermicelli Handling Test: A simple quantitative measure of dexterous forepaw function in rats. *Journal of Neuroscience Methods*, *170*(2), 229–244. <https://doi.org/10.1016/j.jneumeth.2008.01.015>
- Baird, A. L., Meldrum, A., & Dunnett, S. B. (2001). The staircase test of skilled reaching in mice. *Brain Research Bulletin*, *54*(2), 243–250. [https://doi.org/10.1016/S0361-9230\(00\)00457-3](https://doi.org/10.1016/S0361-9230(00)00457-3)
- Bartlett, M. J., Flores, A. J., Ye, T., Smidt, S. I., Dollish, H. K., Stancati, J. A., ... Falk, T. (2020). Preclinical evidence in support of repurposing sub-anesthetic ketamine as a treatment for L-DOPA-induced dyskinesia. *Experimental Neurology*, *333*(July), 113413. <https://doi.org/10.1016/j.expneurol.2020.113413>
- Bartlett, M. J., Joseph, R. M., LePoidevin, L. M., Parent, K. L., Laude, N. D., Lazarus, L. B., ... Falk, T. (2016). Long-term effect of sub-anesthetic ketamine in reducing L-DOPA-induced dyskinesias in a preclinical model. *Neuroscience Letters*, *612*, 121–125. <https://doi.org/10.1016/j.neulet.2015.11.047>
- Berke, J. D., Okatan, M., Skurski, J., & Eichenbaum, H. B. (2004). Oscillatory entrainment of striatal neurons in freely moving rats. *Neuron*, *43*(6), 883–896. <https://doi.org/10.1016/j.neuron.2004.08.035>
- Berman, R. M., Cappiello, A., Anand, A., Oren, D. A., Heninger, G. R., Charney, D. S., & Krystal, J. H. (2000). Antidepressant effects of ketamine in depressed patients. *Biological Psychiatry*, *47*(4), 351–354. [https://doi.org/10.1016/S0006-3223\(99\)00230-9](https://doi.org/10.1016/S0006-3223(99)00230-9)
- Blackwell, A. A., Banovetz, M. T., Qandeel, Whishaw, I. Q., & Wallace, D. G. (2018). The structure of arm and hand movements in a spontaneous and food rewarded on-line string-pulling task by the mouse. *Behavioural Brain Research*, *345*(February), 49–58. <https://doi.org/10.1016/j.bbr.2018.02.025>
- Blackwell, A. A., Köppen, J. R., Whishaw, I. Q., & Wallace, D. G. (2018). String-pulling for food by the rat: Assessment of movement, topography and kinematics of a bilaterally skilled forelimb act. *Learning and Motivation*, *61*(March 2017), 63–73. <https://doi.org/10.1016/j.lmot.2017.03.010>

- Blackwell, A. A., & Wallace, D. G. (2020). Effects of string length on the organization of rat string-pulling behavior. *Animal Cognition*, *23*(2), 415–425. <https://doi.org/10.1007/s10071-020-01349-4>
- Blackwell, A. A., Widick, W. L., Cheatwood, J. L., Wishaw, I. Q., & Wallace, D. G. (2018). Unilateral forelimb sensorimotor cortex devascularization disrupts the topographic and kinematic characteristics of hand movements while string-pulling for food in the rat. *Behavioural Brain Research*, *338*(July 2017), 88–100. <https://doi.org/10.1016/j.bbr.2017.10.014>
- Bonazzi, L., Viaro, R., Lodi, E., Canto, R., Bonifazzi, C., & Franchi, G. (2013). Complex Movement Topography and Extrinsic Space Representation in the Rat Forelimb Motor Cortex as Defined by Long-Duration Intracortical Microstimulation. *The Journal of Neuroscience*, *33*(5), 2097 LP – 2107. <https://doi.org/10.1523/JNEUROSCI.3454-12.2013>
- Braak, H., & Braak, E. (2000). Pathoanatomy of Parkinson's disease. *Journal of Neurology, Supplement*, *247*(2), 3–10. <https://doi.org/10.1007/pl00007758>
- Bragin, A., Jandó, G., Nádasdy, Z., Hetke, J., Wise, K., & Buzsáki, G. (1995). Gamma (40-100 Hz) oscillation in the hippocampus of the behaving rat. *Journal of Neuroscience*, *15*(11), 47–60. <https://doi.org/10.1523/jneurosci.15-01-00047.1995>
- Brazhnik, E., Cruz, A. V., Avila, I., Wahba, M. I., Novikov, N., Ilieva, N. M., ... Walters, J. R. (2012). State-dependent spike and local field synchronization between motor cortex and substantia nigra in hemiparkinsonian rats. *Journal of Neuroscience*, *32*(23), 7869–7880. <https://doi.org/10.1523/JNEUROSCI.0943-12.2012>
- Brown, A. R., & Teskey, G. C. (2014). Motor Cortex is Functionally Organized as a Set of Spatially Distinct Representations for Complex Movements. *Journal of Neuroscience*, *34*(41), 13574–13585. <https://doi.org/10.1523/JNEUROSCI.2500-14.2014>
- Brown, P. (2007). Abnormal oscillatory synchronisation in the motor system leads to impaired movement. *Current Opinion in Neurobiology*, *17*(6), 656–664. <https://doi.org/10.1016/j.conb.2007.12.001>
- Brown, P., Oliviero, A., Mazzone, P., Insola, A., Tonali, P., & Di Lazzaro, V. (2001). Dopamine dependency of oscillations between subthalamic nucleus and pallidum in Parkinson's disease. *Journal of Neuroscience*, *21*(3), 1033–1038. <https://doi.org/10.1523/jneurosci.21-03-01033.2001>

- Brunel, N., & Wang, X. J. (2003). What determines the frequency of fast network oscillations with irregular neural discharges? I. Synaptic dynamics and excitation-inhibition balance. *Journal of Neurophysiology*, *90*(1), 415–430. <https://doi.org/10.1152/jn.01095.2002>
- Buzsáki, G., & Wang, X. J. (2012). Mechanisms of gamma oscillations. *Annual review of neuroscience*, *35*, 203-225.
- Cardin, J. A., Carlén, M., Meletis, K., Knoblich, U., Zhang, F., Deisseroth, K., ... Moore, C. I. (2009). Driving fast-spiking cells induces gamma rhythm and controls sensory responses. *Nature*, *459*(7247), 663–667. <https://doi.org/10.1038/nature08002>
- Carlén, M., Meletis, K., Siegle, J. H., Cardin, J. A., Futai, K., Vierling-Claassen, D., ... Tsai, L. H. (2012). A critical role for NMDA receptors in parvalbumin interneurons for gamma rhythm induction and behavior. *Molecular Psychiatry*, *17*(5), 537–548. <https://doi.org/10.1038/mp.2011.31>
- Cenci, M. A., Jörntell, H., & Petersson, P. (2018). On the neuronal circuitry mediating l-DOPA-induced dyskinesia. *Journal of Neural Transmission*, *125*(8), 1157–1169. <https://doi.org/10.1007/s00702-018-1886-0>
- Chen, M. T., Morales, M., Woodward, D. J., Hoffer, B. J., & Janak, P. H. (2001). In vivo extracellular recording of striatal neurons in the awake rat following unilateral 6-hydroxydopamine lesions. *Experimental Neurology*, *171*(1), 72–83. <https://doi.org/10.1006/exnr.2001.7730>
- Chen, S. Y., & Tsai, S. T. (2010). The epidemiology of Parkinson's disease. *Tzu Chi Medical Journal*, *22*(2), 73–81. [https://doi.org/10.1016/S1016-3190\(10\)60044-4](https://doi.org/10.1016/S1016-3190(10)60044-4)
- Cisek, P., Crammond, D. J., & Kalaska, J. F. (2003). Neural activity in primary motor and dorsal premotor cortex in reaching tasks with the contralateral versus ipsilateral arm. *Journal of Neurophysiology*, *89*(2), 922–942. <https://doi.org/10.1152/jn.00607.2002>
- Cordon, I., Nicolás, M. J., Arrieta, S., Lopetegui, E., López-Azcárate, J., Alegre, M., ... Valencia, M. (2015). Coupling in the cortico-basal ganglia circuit is aberrant in the ketamine model of schizophrenia. *European Neuropsychopharmacology*, *25*(8), 1375–1387. <https://doi.org/10.1016/j.euroneuro.2015.04.004>
- Crocker, A. D. (1997). The regulation of motor control: An evaluation of the role of dopamine receptors in the substantia nigra. *Reviews in the Neurosciences*, *8*(1), 55–76. <https://doi.org/10.1515/REVNEURO.1997.8.1.55>

- Crone, N., Miglioretti, D. L., Gordon, B., & Lesser, R. P. (1998). Functional mapping of human sensorimotor cortex with electrocorticographic spectral analysis. *Brain*, *121*, 2301–2315. Retrieved from <https://academic.oup.com/brain/article-lookup/doi/10.1093/brain/121.12.2301>
- David, H. N., Anseau, M., & Abreini, J. H. (2005). Dopamine-glutamate reciprocal modulation of release and motor responses in the rat caudate-putamen and nucleus accumbens of “intact” animals. *Brain Research Reviews*, *50*(2), 336–360. [https://doi.org/https://doi.org/10.1016/S1471-1931\(00\)00028-8](https://doi.org/https://doi.org/10.1016/S1471-1931(00)00028-8)
- Davie, C. A. (2008). A review of Parkinson’s disease. *British Medical Bulletin*, *86*(1), 109–127. <https://doi.org/10.1093/bmb/ldn013>
- Dejean, C., Gross, C. E., Bioulac, B., & Boraud, T. (2007). Synchronous high-voltage spindles in the cortex-basal ganglia network of awake and unrestrained rats. *European Journal of Neuroscience*, *25*(3), 772–784. <https://doi.org/10.1111/j.1460-9568.2007.05305.x>
- Domino, E. F., Chodoff, P., & Corssen, G. (1965). Pharmacologic effects of CI-581, a new dissociative anesthetic, in man. *Clinical Pharmacology and Therapeutics*, *6*(3), 279–291. <https://doi.org/10.1002/cpt196563279>
- Duman, R. S., Aghajanian, G. K., Sanacora, G., & Krystal, J. H. (2016). Synaptic plasticity and depression: New insights from stress and rapid-acting antidepressants. *Nature Medicine*, *22*(3), 238–249. <https://doi.org/10.1038/nm.4050>
- Duman, R. S., & Aghajanian, G. K. (2012). Synaptic Dysfunction in Depression: Potential Therapeutic Targets. *Science*, *338*(6103), 68 LP – 72. <https://doi.org/10.1126/science.1222939>
- Dvorak, D., & Fenton, A. A. (2014). Toward a proper estimation of phase-amplitude coupling in neural oscillations. *Journal of Neuroscience Methods*, *225*, 42–56. <https://doi.org/10.1016/j.jneumeth.2014.01.002>
- Economo, M. N., Viswanathan, S., Tasic, B., Bas, E., Winnubst, J., Menon, V., ... Svoboda, K. (2018). Distinct descending motor cortex pathways and their roles in movement. *Nature*, *563*(7729), 79–84. <https://doi.org/10.1038/s41586-018-0642-9>
- Egelman, D. M., Person, C., & Montague, P. R. (1998). A computational role for dopamine delivery in human decision-making. *Journal of Cognitive Neuroscience*, *10*(5), 623–630. <https://doi.org/10.1162/089892998563022>

- Ellens, D. J., & Leventhal, D. K. (2013). Electrophysiology of basal ganglia and cortex in models of parkinson disease. *Journal of Parkinson's Disease*, 3(3), 241–254. <https://doi.org/10.3233/JPD-130204>
- Ferguson, B. R., & Gao, W. J. (2018). Pv interneurons: critical regulators of E/I balance for prefrontal cortex-dependent behavior and psychiatric disorders. *Frontiers in Neural Circuits*, 12(May), 1–13. <https://doi.org/10.3389/fncir.2018.00037>
- Fisher, N. I. (1995). *Statistical analysis of circular data*. Cambridge university press.
- Fukumoto, K., Iijima, M., & Chaki, S. (2016). The Antidepressant Effects of an mGlu2/3 Receptor Antagonist and Ketamine Require AMPA Receptor Stimulation in the mPFC and Subsequent Activation of the 5-HT Neurons in the DRN. *Neuropsychopharmacology*, 41(4), 1046–1056. <https://doi.org/10.1038/npp.2015.233>
- Gandal, M. J., Sisti, J., Klook, K., Ortinski, P. I., Leitman, V., Liang, Y., ... Siegel, S. J. (2012). GABA B-mediated rescue of altered excitatory-inhibitory balance, gamma synchrony and behavioral deficits following constitutive NMDAR-hypofunction. *Translational Psychiatry*, 2(December 2011). <https://doi.org/10.1038/tp.2012.69>
- Ge, S., Yang, C., Li, M., Li, J., Chang, X., Fu, J., ... Gao, G. (2012). Dopamine depletion increases the power and coherence of high-voltage spindles in the globus pallidus and motor cortex of freely moving rats. *Brain Research*, 1465, 66–79. <https://doi.org/10.1016/j.brainres.2012.05.002>
- Girasole, A. E., Lum, M. Y., Nathaniel, D., Bair-Marshall, C. J., Guenther, C. J., Luo, L., ... Nelson, A. B. (2018). A Subpopulation of Striatal Neurons Mediates Levodopa-Induced Dyskinesia. *Neuron*, 97(4), 787-795.e6. <https://doi.org/10.1016/j.neuron.2018.01.017>
- Goldberg, J. A., Boraud, T., Maraton, S., Haber, S. N., Vaadia, E., & Bergman, H. (2002). Enhanced Synchrony among Primary Motor Cortex Neurons in the 1-Methyl-4-Phenyl-1,2,3,6-Tetrahydropyridine Primate Model of Parkinson's Disease. *Journal of Neuroscience*, 22(11), 4639–4653. <https://doi.org/10.1523/jneurosci.22-11-04639.2002>
- Guyon, N., Zacharias, L. R., de Oliveira, E. F., Kim, H., Leite, J. P., Lopes-Aguiar, C., & Carlén, M. (2021). Network asynchrony underlying increased broadband gamma power. *Journal of Neuroscience*, 41(13), 2944-2963. <https://doi.org/10.1523/JNEUROSCI.2250-20.2021>
- Gyorgy, B., & Andreas, D. (2004). Neuronal Oscillations in Cortical Networks. *Science*, 304(June), 1926–1929. Retrieved from <http://science.sciencemag.org/>

- Halje, P., Tamtè, M., Richter, U., Mohammed, M., Angela Cenci, M., & Petersson, P. (2012). Levodopa-induced dyskinesia is strongly associated with resonant cortical oscillations. *Journal of Neuroscience*, *32*(47), 16541–16551. <https://doi.org/10.1523/JNEUROSCI.3047-12.2012>
- Hammond, C., Bergman, H., & Brown, P. (2007). Pathological synchronization in Parkinson's disease: networks, models and treatments. *Trends in Neurosciences*, *30*(7), 357–364. <https://doi.org/10.1016/j.tins.2007.05.004>
- Heinrich, B. (1995). An Experimental Investigation of Insight in Common Ravens (*Corvus corax*). *The Auk*, *112*(4), 994–1003. Retrieved from <http://www.jstor.org/stable/4089030>
- Hirota, K., & Lambert, D. G. (1996). Ketamine: Its mechanism(s) of action and unusual clinical uses. *British Journal of Anaesthesia*, *77*(4), 441–444. <https://doi.org/10.1093/bja/77.4.441>
- Hudson, M. R., Sokolenko, E., O'Brien, T. J., & Jones, N. C. (2020). NMDA receptors on parvalbumin-positive interneurons and pyramidal neurons both contribute to MK-801 induced gamma oscillatory disturbances: Complex relationships with behaviour. *Neurobiology of Disease*, *134*(September 2019), 104625. <https://doi.org/10.1016/j.nbd.2019.104625>
- Hunt, M. J., Falinska, M., Łęski, S., Wójcik, D. K., & Kasicki, S. (2011). Differential effects produced by ketamine on oscillatory activity recorded in the rat hippocampus, dorsal striatum and nucleus accumbens. *Journal of Psychopharmacology*, *25*(6), 808–821. <https://doi.org/10.1177/0269881110362126>
- Inayat, S., Singh, S., Ghasroddashti, A., Qandeel, Egodage, P., Wishaw, I. Q., & Mohajerani, M. H. (2020). A matlab-based toolbox for characterizing behavior of rodents engaged in string-pulling. *ELife*, *9*, 1–31. <https://doi.org/10.7554/eLife.54540>
- Jacobs, I. F., & Osvath, M. (2015). The string-pulling paradigm in comparative psychology. *Journal of Comparative Psychology*, *129*(2), 89–120. <https://doi.org/10.1037/a0038746>
- Jenkinson, N., & Brown, P. (2011). New insights into the relationship between dopamine, beta oscillations and motor function. *Trends in Neurosciences*, *34*(12), 611–618. <https://doi.org/10.1016/j.tins.2011.09.003>
- Jenkinson, N., & Brown, P. (2011). New insights into the relationship between dopamine, beta oscillations and motor function. *Trends in Neurosciences*, *34*(12), 611–618. <https://doi.org/10.1016/j.tins.2011.09.003>

- Jenkinson, N., & Brown, P. (2011). New insights into the relationship between dopamine, beta oscillations and motor function. *Trends in Neurosciences*, *34*(12), 611–618. <https://doi.org/10.1016/j.tins.2011.09.003>
- Jenner, P. (2008). Molecular mechanisms of L-DOPA-induced dyskinesia. *Nature Reviews Neuroscience*, *9*(9), 665–677. <https://doi.org/10.1038/nrn2471>
- Jensen, O., & Colgin, L. L. (2007). Cross-frequency coupling between neuronal oscillations. *Trends in Cognitive Sciences*, *11*(7), 267–269. <https://doi.org/10.1016/j.tics.2007.05.003>
- Jin, X., Schwabe, K., Krauss, J. K., & Alam, M. (2016). Coherence of neuronal firing of the entopeduncular nucleus with motor cortex oscillatory activity in the 6-OHDA rat model of Parkinson's disease with levodopa-induced dyskinesias. *Experimental Brain Research*, *234*(4), 1105–1118. <https://doi.org/10.1007/s00221-015-4532-1>
- Johnson, S. W., Seutin, V., & North, R. A. (1992). Burst firing in dopamine neurons induced by N-methyl-D-aspartate: Role of electrogenic sodium pump. *Science*, *258*(5082), 665–667. <https://doi.org/10.1126/science.1329209>
- Kocsis, B. (2012). Differential role of NR2A and NR2B subunits in N-methyl-D-aspartate receptor antagonist-induced aberrant cortical gamma oscillations. *Biological Psychiatry*, *71*(11), 987–995. <https://doi.org/10.1016/j.biopsych.2011.10.002>
- Kühn, A. A., Tsui, A., Aziz, T., Ray, N., Brücke, C., Kupsch, A., ... Brown, P. (2009). Pathological synchronisation in the subthalamic nucleus of patients with Parkinson's disease relates to both bradykinesia and rigidity. *Experimental Neurology*, *215*(2), 380–387. <https://doi.org/10.1016/j.expneurol.2008.11.008>
- Kurniawan, I. T., Guitart-Masip, M., & Dolan, R. J. (2011). Dopamine and effort-based decision making. *Frontiers in Neuroscience*, *5*(JUN), 1–10. <https://doi.org/10.3389/fnins.2011.00081>
- Krystal, J. H., Karper, L. P., Seibyl, J. P., Freeman, G. K., Delaney, R., Bremner, D., Heninger, G. R., Bowers, M. B. (1994). Subanesthetic Effects of the Noncompetitive NMDA Antagonist, Ketamine, in Humans. *Archives of General Psychiatry*, *51*(3), 199–214. <https://doi.org/10.1001/archpsyc.1994.03950030035004>
- Lara, A. H., Cunningham, J. P., & Churchland, M. M. (2018). Different population dynamics in the supplementary motor area and motor cortex during reaching. *Nature Communications*, *9*(1). <https://doi.org/10.1038/s41467-018-05146-z>

- Lauritsen, C., Mazuera, S., Lipton, R. B., & Ashina, S. (2016). Intravenous ketamine for subacute treatment of refractory chronic migraine: a case series. *Journal of Headache and Pain*, *17*(1), 4–8. <https://doi.org/10.1186/s10194-016-0700-3>
- Lazarewicz, M. T., Ehrlichman, R. S., Maxwell, C. R., Gandal, M. J., Finkel, L. H., & Siegel, S. J. (2010). Ketamine modulates theta and gamma oscillations. *Journal of Cognitive Neuroscience*, *22*(7), 1452–1464. <https://doi.org/10.1162/jocn.2009.21305>
- Li, N., Lee, B., Liu, R.-J., Banasr, M., Dwyer, J. M., Iwata, M., ... Duman, R. S. (2010). mTOR-Dependent Synapse Formation Underlies the Rapid Antidepressant Effects of NMDA Antagonists. *Science*, *329*(5994), 959 LP – 964. <https://doi.org/10.1126/science.1190287>
- Liriano, F., Hatten, C., & Schwartz, T. L. (2019). Ketamine as treatment for post-traumatic stress disorder: A review. *Drugs in Context*, *8*, 1–7. <https://doi.org/10.7573/dic.212305>
- Lisman, J. E. (1997). Bursts as a unit of neural information: Making unreliable synapses reliable. *Trends in Neurosciences*, *20*(1), 38–43. [https://doi.org/10.1016/S0166-2236\(96\)10070-9](https://doi.org/10.1016/S0166-2236(96)10070-9)
- Little, S., & Brown, P. (2014). The functional role of beta oscillations in Parkinson's disease. *Parkinsonism and Related Disorders*, *20*(SUPPL.1), S44–S48. [https://doi.org/10.1016/S1353-8020\(13\)70013-0](https://doi.org/10.1016/S1353-8020(13)70013-0)
- Liu, R. J., Lee, F. S., Li, X. Y., Bambico, F., Duman, R. S., & Aghajanian, G. K. (2012). Brain-derived neurotrophic factor Val66Met allele impairs basal and ketamine-stimulated synaptogenesis in prefrontal cortex. *Biological Psychiatry*, *71*(11), 996–1005. <https://doi.org/10.1016/j.biopsych.2011.09.030>
- Lobb, C. J. (2014). Abnormal bursting as a pathophysiological mechanism in Parkinson's disease. *Basal Ganglia*, *3*(4), 187–195. <https://doi.org/10.1016/j.baga.2013.11.002>
- Luft, A. R., & Schwarz, S. (2009). Dopaminergic signals in primary motor cortex. *International Journal of Developmental Neuroscience*, *27*(5), 415–421. <https://doi.org/10.1016/j.ijdevneu.2009.05.004>
- Mathis, A., Mamidanna, P., Cury, K. M., Abe, T., Murthy, V. N., Mathis, M. W., & Bethge, M. (2018). DeepLabCut: markerless pose estimation of user-defined body parts with deep learning. *Nature Neuroscience*, *21*(9), 1281–1289. <https://doi.org/10.1038/s41593-018-0209-y>
- McNally, J. M., McCarley, R. W., McKenna, J. T., Yanagawa, Y., & Brown, R. E. (2011). Complex receptor mediation of acute ketamine application on in vitro gamma oscillations in mouse

- prefrontal cortex: Modeling gamma band oscillation abnormalities in schizophrenia. *Neuroscience*, 199, 51–63. <https://doi.org/10.1016/j.neuroscience.2011.10.015>
- McNally, J. M., Aguilar, D. D., Katsuki, F., Radzik, L. K., Schiffino, F. L., Uygun, D. S., ... Brown, R. E. (2020). Optogenetic manipulation of an ascending arousal system tunes cortical broadband gamma power and reveals functional deficits relevant to schizophrenia. *Molecular Psychiatry*. <https://doi.org/10.1038/s41380-020-0840-3>
- Mirenowicz, J., & Schultz, W. (1994). Importance of unpredictability for reward responses in primate dopamine neurons. *Journal of Neurophysiology*, 72(2), 1024–1027. <https://doi.org/10.1152/jn.1994.72.2.1024>
- Nitsche, M. A., Lampe, C., Antal, A., Liebetanz, D., Lang, N., Tergau, F., & Paulus, W. (2006). Dopaminergic modulation of long-lasting direct current-induced cortical excitability changes in the human motor cortex. *European Journal of Neuroscience*, 23(6), 1651–1657. <https://doi.org/10.1111/j.1460-9568.2006.04676.x>
- Obeso, J. A., Rodriguez-Oroz, M. C., Rodriguez, M., Lanciego, J. L., Artieda, J., Gonzalo, N., & Olanow, C. W. (2000). Pathophysiology of the basal ganglia in Parkinson's disease. *Trends in Neurosciences*, 23(Box 1), S8–S19. [https://doi.org/10.1016/S1471-1931\(00\)00028-8](https://doi.org/10.1016/S1471-1931(00)00028-8)
- Pasquereau, B., & Turner, R. S. (2011). Primary motor cortex of the parkinsonian monkey: Differential effects on the spontaneous activity of pyramidal tract-type neurons. *Cerebral Cortex*, 21(6), 1362–1378. <https://doi.org/10.1093/cercor/bhq217>
- Pfurtscheller, G., Graftmann, B., Huggins, J. E., Levine, S. P., & Schuh, L. A. (2003). Spatiotemporal patterns of beta desynchronization and gamma synchronization in corticographic data during self-paced movement. *Clinical Neurophysiology*, 114(7), 1226–1236. [https://doi.org/10.1016/S1388-2457\(03\)00067-1](https://doi.org/10.1016/S1388-2457(03)00067-1)
- Pinault, D. (2008). N-Methyl d-Aspartate Receptor Antagonists Ketamine and MK-801 Induce Wake-Related Aberrant γ Oscillations in the Rat Neocortex. *Biological Psychiatry*, 63(8), 730–735. <https://doi.org/10.1016/j.biopsych.2007.10.006>
- Porter, B., & Hillman, K. L. (2019). A Novel Weight Lifting Task for Investigating Effort and Persistence in Rats. *Frontiers in Behavioral Neuroscience*, 13(December), 1–13. <https://doi.org/10.3389/fnbeh.2019.00275>
- Rao, V. R., & Lowenstein, D. H. (2015). Epilepsy. *Current Biology*, 25(17), R742–R746. <https://doi.org/10.1016/j.cub.2015.07.072>

- Reddi, D. (2016). Preventing chronic postoperative pain. *Anaesthesia*, 71, 64–71.
<https://doi.org/10.1111/anae.13306>
- Richter, U., Halje, P., & Petersson, P. (2013). Mechanisms underlying cortical resonant states: Implications for levodopa-induced dyskinesia. *Reviews in the Neurosciences*, 24(4), 415–429. <https://doi.org/10.1515/revneuro-2013-0018>
- Romo, R., & Schultz, W. (1990). Dopamine neurons of the monkey midbrain: Contingencies of responses to active touch during self-initiated arm movements. *Journal of Neurophysiology*, 63(3), 592–606. <https://doi.org/10.1152/jn.1990.63.3.592>
- Ronald S Duman, George K Aghajanian, G. S. & J. H. K. (2016). Synaptic plasticity and depression: new insights from stress and rapid-acting antidepressants. *Physiology & Behavior*, 22(3). <https://doi.org/10.1038/nm.4050>.Synaptic
- Sabol, K. E., Richards, J. B., & Freed, C. R. (1990). In vivo dialysis measurements of dopamine and DOPAC in rats trained to turn on a circular treadmill. *Pharmacology, Biochemistry and Behavior*, 36(1), 21–28. [https://doi.org/10.1016/0091-3057\(90\)90119-3](https://doi.org/10.1016/0091-3057(90)90119-3)
- Santos-Lobato, B. L., Schumacher-Schuh, A. F., Rieder, C. R. M., Hutz, M. H., Borges, V., Ferraz, H. B., ... Tumas, V. (2020). Diagnostic prediction model for levodopa-induced dyskinesia in Parkinson's disease. *Arquivos de Neuro-Psiquiatria*, 78(4), 206–216.
<https://doi.org/10.1590/0004-282X20190191>
- Shaw, A. D., Saxena, N., Jackson, L. E., Hall, J. E., Singh, K. D., & Muthukumaraswamy, S. D. (2015). Ketamine amplifies induced gamma frequency oscillations in the human cerebral cortex. *European Neuropsychopharmacology*, 25(8), 1136–1146.
<https://doi.org/10.1016/j.euroneuro.2015.04.012>
- Shen, G., Han, F., & Shi, W. X. (2018). Effects of Low Doses of Ketamine on Pyramidal Neurons in Rat Prefrontal Cortex. *Neuroscience*, 384, 178–187.
<https://doi.org/10.1016/j.neuroscience.2018.05.037>
- Shen, L., & Alexander, G. E. (1997). Preferential representation of instructed target location versus limb trajectory in dorsal premotor area. *Journal of Neurophysiology*, 77(3), 1195–1212. <https://doi.org/10.1152/jn.1997.77.3.1195>
- Shenoy, K. V., Sahani, M., & Churchland, M. M. (2013). Cortical control of arm movements: A dynamical systems perspective. *Annual Review of Neuroscience*, 36, 337–359.
<https://doi.org/10.1146/annurev-neuro-062111-150509>

- Shinomoto, S., Shima, K., & Tanji, J. (2003). Differences in Spiking Patterns among Cortical Neurons. *Neural Computation*, *15*(12), 2823–2842.
<https://doi.org/10.1162/089976603322518759>
- Singh, F., Shu, I. W., Hsu, S. H., Link, P., Pineda, J. A., & Granholm, E. (2020). Modulation of frontal gamma oscillations improves working memory in schizophrenia. *NeuroImage: Clinical*, *27*(February), 102339. <https://doi.org/10.1016/j.nicl.2020.102339>
- Singh, S., Mandziak, A., Barr, K., Blackwell, A. A., Mohajerani, M. H., Wallace, D. G., & Wishaw, I. Q. (2019). Human string-pulling with and without a string: movement, sensory control, and memory. *Experimental Brain Research*, *237*(12), 3431–3447.
<https://doi.org/10.1007/s00221-019-05684-y>
- Slovik, M., Rosin, B., Moshel, S., Mitelman, R., Schechtman, E., Eitan, R., ... Bergman, H. (2017). Ketamine induced converged synchronous gamma oscillations in the cortico-basal ganglia network of nonhuman primates. *Journal of Neurophysiology*, *118*(2), 917–931.
<https://doi.org/10.1152/jn.00765.2016>
- Sohal, V. S., & Rubenstein, J. L. R. (2019). Excitation-inhibition balance as a framework for investigating mechanisms in neuropsychiatric disorders. *Molecular Psychiatry*, *24*(9), 1248–1257. <https://doi.org/10.1038/s41380-019-0426-0>
- Syed, E. C. J., Grima, L. L., Magill, P. J., Bogacz, R., Brown, P., & Walton, M. E. (2015). Action initiation shapes mesolimbic dopamine encoding of future rewards. *Nature Neuroscience*, *19*(1), 34–36. <https://doi.org/10.1038/nn.4187>
- Tamtè, M., Brys, I., Richter, U., Ivica, N., Halje, P., & Petersson, P. (2016). Systems-level neurophysiological state characteristics for drug evaluation in an animal model of levodopa-induced dyskinesia. *Journal of Neurophysiology*, *115*(3), 1713–1729.
<https://doi.org/10.1152/jn.00868.2015>
- Tennant, K. A., Asay, A. L., Allred, R. P., Ozburn, A. R., Kleim, J. A., & Jones, T. A. (2010). The vermicelli and capellini handling tests: Simple quantitative measures of dexterous forepaw function in rats and mice. *Journal of Visualized Experiments*, (41), 1–5.
<https://doi.org/10.3791/2076>
- Underwood, C. F., & Parr-Brownlie, L. C. (2021). Primary motor cortex in Parkinson's disease: Functional changes and opportunities for neurostimulation. *Neurobiology of Disease*, *147*, 105159. <https://doi.org/10.1016/j.nbd.2020.105159>

- Wahyu Indriani, D., Chiken, S., Hasegawa, T., Sano, H., & Nambu, A. (2021). Abnormal cortico-basal ganglia neurotransmission in a mouse model of l-DOPA-induced dyskinesia. *The Journal of Neuroscience*, *41*(12), JN-RM-0267-20. <https://doi.org/10.1523/jneurosci.0267-20.2020>
- Weinberger, M., Mahant, N., Hutchison, W. D., Lozano, A. M., Moro, E., Hodaie, M., ... Dostrovsky, J. O. (2006). Beta oscillatory activity in the subthalamic nucleus and its relation to dopaminergic response in Parkinson's disease. *Journal of Neurophysiology*, *96*(6), 3248–3256. <https://doi.org/10.1152/jn.00697.2006>
- Whishaw, I. Q. (1996). An endpoint, descriptive, and kinematic comparison of skilled reaching in mice (*Mus musculus*) with rats (*Rattus norvegicus*). *Behavioural Brain Research*, *78*(2), 101–111. [https://doi.org/10.1016/0166-4328\(95\)00236-7](https://doi.org/10.1016/0166-4328(95)00236-7)
- Whishaw, I. Q., & Coles, B. L. K. (1996). Varieties of paw and digit movement during spontaneous food handling in rats: Postures, bimanual coordination, preferences, and the effect of forelimb cortex lesions. *Behavioural Brain Research*, *77*(1–2), 135–148. [https://doi.org/10.1016/0166-4328\(95\)00209-X](https://doi.org/10.1016/0166-4328(95)00209-X)
- Whishaw, I. Q., Pellis, S. M., Gorny, B. P., & Pellis, V. C. (1991). The impairments in reaching and the movements of compensation in rats with motor cortex lesions: an endpoint, videorecording, and movement notation analysis. *Behavioural Brain Research*, *42*(1), 77–91. [https://doi.org/10.1016/S0166-4328\(05\)80042-7](https://doi.org/10.1016/S0166-4328(05)80042-7)
- Wise, R. A. (2004). Dopamine, learning and motivation. *Nature Reviews Neuroscience*, *5*(6), 483–494. <https://doi.org/10.1038/nrn1406>
- Wu, M., Minkowicz, S., Dumrongprechachan, V., Hamilton, P., & Kozorovitskiy, Y. (2021). Ketamine rapidly enhances glutamate-evoked dendritic spinogenesis in medial prefrontal cortex through dopaminergic mechanisms. *Biological Psychiatry*. <https://doi.org/10.1016/j.biopsych.2020.12.022>
- Yang, C., Ge, S. N., Zhang, J. R., Chen, L., Yan, Z. Q., Heng, L. J., ... Gao, G. D. (2013). Systemic Blockade of Dopamine D2-Like Receptors Increases High-Voltage Spindles in the Globus Pallidus and Motor Cortex of Freely Moving Rats. *PLoS ONE*, *8*(6). <https://doi.org/10.1371/journal.pone.0064637>
- Yang, Y., Cui, Y., Sang, K., Dong, Y., Ni, Z., Ma, S., & Hu, H. (2018). Ketamine blocks bursting in the lateral habenula to rapidly relieve depression. *Nature*, *554*(7692), 317–322. <https://doi.org/10.1038/nature25509>

Ye, T., Bartlett, M. J., Schmit, M. B., Sherman, S. J., Falk, T., & Cowen, S. L. (2018). Ten-Hour Exposure to Low-Dose Ketamine Enhances Corticostriatal Cross-Frequency Coupling and Hippocampal Broad-Band Gamma Oscillations. *Frontiers in Neural Circuits*, *12*(August), 1–16. <https://doi.org/10.3389/fncir.2018.00061>

Ye, T., Bartlett, M. J., Sherman, S. J., Falk, T., & Cowen, S. L. (2021). Spectral signatures of L-DOPA-induced dyskinesia depend on L-DOPA dose and are suppressed by ketamine. *Experimental Neurology*, *340*(February), 113670. <https://doi.org/10.1016/j.expneurol.2021.113670>

Zhang, X., Feng, Z. J., & Chergui, K. (2014). GluN2D-containing NMDA receptors inhibit neurotransmission in the mouse striatum through a cholinergic mechanism: Implication for Parkinson's disease. *Journal of Neurochemistry*, *129*(4), 581–590. <https://doi.org/10.1111/jnc.12658821>. <https://doi.org/10.1177/02698811110362126>